UNIVERSITA' DEGLI STUDI DI PADOVA

DIPARTIMENTO DI INGEGNERIA CIVILE EDILE E AMBIENTALE

CORSO DI LAUREA MAGISTRALE IN INGEGNERIA CIVILE

Tesi di Laurea Magistrale in Ingegneria Civile Strutturale

CONSTITUTIVE MODELLING OF FIBRE REINFORCED CONCRETE

Relatore Italiano: Prof. Francesco Pesavento
Co-Relatore Italiano: Prof. Bernhard Schrefler
Co-Relatore Estero: Prof. Tony Jefferson

Contro-Relatore:Prof. Lorenzo Sanavia

Lureando: MATTEO PARISE

ANNO ACCADEMICO 2013/2014

...con la speranza che sia d'aiuto o ispirazione
per approfondimenti successivi...

Contents

Introduction

The present thesis considers the behaviour of fibre reinforced concrete. Its primary focus is the study and development of mechanics-based numerical models to describe this behaviour. The main motivations for this study are the need for a comprehensive model that would capture the characteristic behaviour of fibre-reinforced composites. The importance and potential of this material in construction industry makes this material interesting. This importance is due to a cheap material necessity, like concrete, but with ductile behaviour and tensile strength, like steel. The aim of this work is twofold. The first is improve a FRC numerical model for straight fibres. The second is to realize a FRC numerical model for hooked ends fibres. Thus the thesis is subdivide in 2 parts. The first part is about FRC with straight fibres. The different chapters introduce at the FRC general knowledge, they describe the numerical model used and, subsequently, they talk about analysis and studies done to improve the Lin and Li model. These analysis are mainly about probability functions of fibre orientation angle and distribution. The second part talks about FRC with hooked ends fibres. In particular it is developed an analytical model able to simulate the fibre pull-out test behaviour. This model starts from some simple mechanic relationship and use the small deformation theory. Indeed it is the only model with this type of premise. Experimental data comparisons and FEM modelling are used to validate the model. At the treatise end is present a paragraph where the main model advantages and disadvantages are described. In particular they are described some key-points for the model improving. With this thesis is reached a better FRC with straight fibres knowledge. In particular it was improve the fibres probability distribution and orientation’s function knowledge. Nevertheless the model developed for the hooked ends fibres is really important mainly for future improving or implementation in a FEM code.

Riassunto

Il lavoro di tesi svolto in questo elaborato tratta la modellazione e lo studio del calcestruzzo fibro-rinforzato. L'elaborato é suddiviso in una prima parte che verte sulla descrizione e sulla conoscenza attuale del FRC. Da questo punto di vista é stato svolto uno studio sui parametri e sui valori tipici del composto in questione. Lo studio si é poi spostato in direzione di approfondire aspetti non ancora chiari o particolarmente approfonditi in questo campo. In particolare si é analizzato il comportamento meccanico dell'interfaccia fibra-matrice cementizia e la distribuzione probabilistica dell'orientazione e distribuzione delle fibre all'interno del composto. Per tutte queste analisi é stato usato il modello analitico proposto da Lin e Li, mediante uno script con il software commerciale Mathcad. La seconda parte tratta la modellazione del FRC qualora si utilizzino fibre con estremità uncinate. un modello analitico é stato creato a partire da relazioni meccaniche basate sulla teoria degli piccoli spostamenti. Si é poi osservato che quest'ultimo é in grado di descrivere in maniera soddisfacente il comportamento di un test di trazione su singola fibra. é stata svolta anche una semplice analisi al FEM per validare e capire alcuni meccanismi che avvengono durante un test di trazione su fibra. Una volta completato il tutto é stato creato uno script in Mathcad in grado di simulare il fenomeno.

Chapter 1

Fibre reinforced concrete

In this chapter is described the general characteristic of fibre reinforced concrete (FRC) and the Knowledge level of this compound.

1.1 General characteristic

Concrete is a material widely used in Engineering for its mechanical characteristics, resistance, chemical behaviour and economic availability. Like in every material there are some advantages and some disadvantages. Two of the biggest disadvantages of concrete are its tensile behaviour and its quasi-brittle behaviour, indeed it has a tensile strength quite smaller than others materials and the post peak branch has a soft hardening trend. To improve the last two and others characteristic like limitation of the micro-cracks propagation (with consequently improving of the structure durability), energy absorption (ideal for seismic application), peak tension value and others, it is possible to mix in a cementitious matrix, randomly distributed short fibres that can be made of various materials such as steel, plastic or natural ones, with the result shown in Fig.1.1a, Fig.1.1b.

Fig.1.1a *Test specimen of fibre reinforced concrete*

Fig.1.1b *Different types of fibres for FRC*

FRC is a mix of 2 different materials, therefore its behaviour depends not only on the mechanical characteristics of the matrix but also on the mechanical/physical characteristics of the fibres. The typical physical and geometric values to represent the fibre contribute are shown in table 1.1.

Table 1.1 *Mains fibre parameters in FRC*

Name	Symbol	Measurement Unit	Range of value
Volume fraction of the fibres	V_f	/	0.5 - 8 %
Fibre length	L_f	mm	20 - 70
Fibre diameter	D_f	mm	0.2 - 1
Aspect ratio	L_f/d_f	/	20 - 300
Young's Modulus	E_f	MPa	20000 - 200000

Some of the possible used of FRC are:

- In design phase for pre-cast structures to improve the durability, hindering the micro cracking propagation
- In design phase to improve the structure ductility and peak load resistance
- In extraordinary maintenance to warranty a minimum of ductility/resistance.

Nevertheless, the economical aspects need to be taken into account in the use of FRC.

The uses in civil engineering describe above come of the benefits from using fibres in a concrete mix, in particular these benefits are:

- increase of toughness or ductility
- increase of durability
- increase of tensile strength
- increase of compression strength

1.1.1 Ductile behaviour

One of the main identification characteristic of the FRC is its ability to give a ductile post-peak behaviour. The slope of the post-peak branch in the stress-strain curve depends upon the proprieties of the components incorporated in the composite: volume fraction, aspect ratio, Young's modulus of the fibres, Young's modulus of the matrix; and the range of variability is very large as is shown in Fig.1.4.

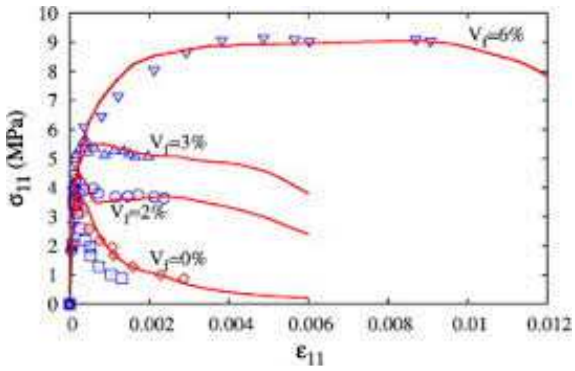

Fig.1.2 *Experimentally data that shown the variability of the branch slope after the force peak*

It is very important to remember the physical meaning of the area under the graph. This area represents the compound work so it is directly linked to the energy absorption, necessary to avoid brittle and instant rupture. Obviously the post-peak behaviour depends on many factors and the figure above describes a general trend obtained with the insertion of fibres.

1.1.2 Durability improvement

The structural durability is grow of importance in the last years, indeed numbers of studies about prediction and delay of structure decay for durability factors are enhance. One of the most important aspects in the concrete structures durability is the presence of fracture in the concrete matrix. Limitation of fracture presence or development it allows to protect the inner reinforce bars from corrosion and chemical attack thus maintain the original mechanical characteristics. The presence of short randomly distributed fibres increase both the aspect above mentioned. The first benefit effect is given by delay the crack formation because the FRC has a tensile strength bigger than the plain concrete. The second benefit come from the ductile behaviour of FRC that avoid/decrease the development of fractures because it require a force increasing for the crack width development.

1.1.3 Effect on tensile and compressive strength

FRC benefit about the force peak resistance is notable in the compression strength (Fig.1.2) as well as in the tension strength (Fig.1.3), even if the magnitude of enhance is bigger for the tension strength than for the compression, how is expected for a material like concrete.

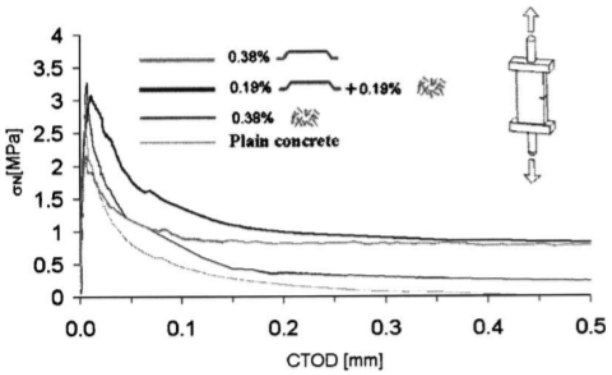

Fig.1.3 *[2]Enhance of tension strength over variation of fibre volume fraction*

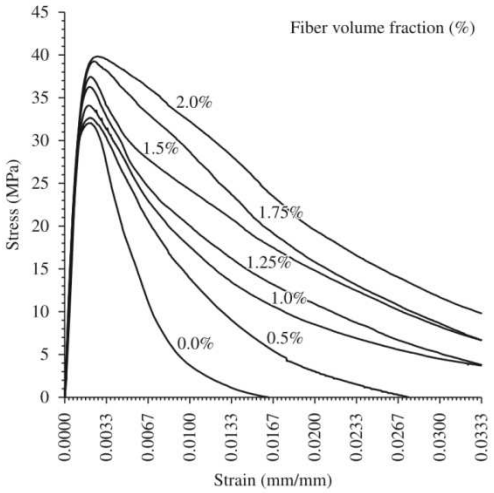

Fig.1.4 *[3]Enhance of compressive strength over variation of fibre volume fraction*

As is possible to see above in the tension case (Fig.1.3) the increase relative to the plain concrete is in the order of 70-80%, hence 7-8 times higher than for the compressive tension case. Nevertheless the important increasing of the peak load, the use of FRC is not just for this purpose, but, is keep in account in design phase.

1.2 Hooked ends

To improve the mains benefits of FRC is possible intervene in two ways. One way is improve the materials characteristics like strength or bond resistance [8], e.g. changing w/c rapport, inserting silica fume. This first way is more link to the matrix than to the fibres. Another direction is change the geometry of the fibres. In the second one, in the last years, some authors studied the behaviour of the cementitious composites with short randomly distributed fibres having hooked ends. Hence are used not straight ends fibres with the purpose of have a better anchorage to the cementitious matrix.

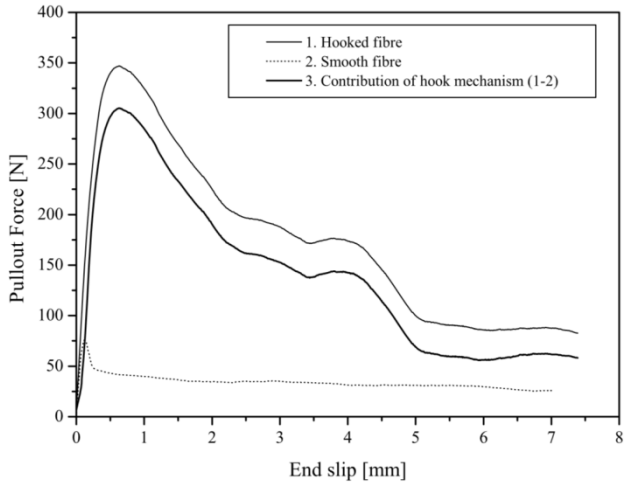

Fig.1.5 *Pull-out test with smooth fibre and fibre with hooked end*

How is possible to see from the figure above (Fig. 1.5) the benefits of the hooked ends are quite relevant. The behaviour improvement is in term of strength and in term of ductility as well, these enhances are for all the commons hook geometry. The hook geometry has to guaranty enhance of the composite proprieties but, at the same time, it has to avoid a quasi-brittle breaks. For these reasons the mains shapes are the same (Fig. 1.6/1.7) and the variability is link to the length parameters (Fig.1.8).

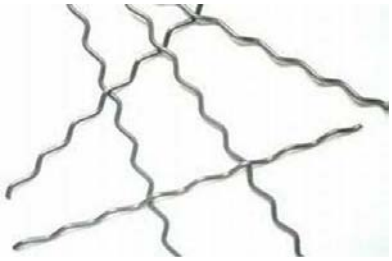

Fig. 1.6

Fig. 1.7

Mains commercial types of fibres shape

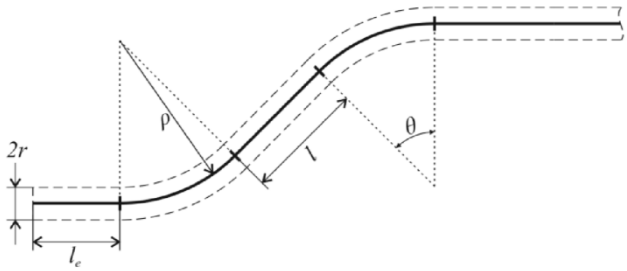

Fig.1.8 *Mains geometrical parameters of fibre shape*

The hooked ends increase the energy necessary to the pull-out force using the energy necessary to straighten the hooks. The mains energy resource due to the hooks are:

- necessity of energy to bend the hooks
- presence of peak contact friction force in the hook place

The hooked ends fibres haven't particular disadvantages if not only for the more complication and difficulty present in the models used to describe them behaviour.

1.3 Knowledge level

FRC compounds are studied for the last 20 years to find a model that describe as good as possible the behaviour of elements build with this material. To increase the potentiality of fibre reinforced concrete were developed particulars type of compound called Engineered cementitious composites (ECC). This fibres-mortar mixes are characterized by a very sharp study of the minimum detail to use the max potential of both the compound's materials (fibres and cementitious matrix). Empirical models were developed to recreate the behaviour of FRC specimens fitting experimentally data. Nevertheless the biggest interest of the research is in the field of matrix-fibre interface interaction. They were created mathematical models with different mains hypothesis. Even models that consider shrinkage, thermal dilatation, the effect of Poisson coefficient and others [4][5]. With the developed of FEM analysis the research has been widen also in this direction. It was created particular finite elements to describe the matrix-fibre interaction, software to recreate a randomly fibres distribution and mechanical/energetic analysis of fibre pull-out. One of the bigger differences of the several FRC models is in the constitutive law used to describe the relationship between friction tensions (usually called "τ") and the displacement during bonding/debonding stage (usually represented by the fibre slip "δ"). Indeed models foresee e.g. τ-constant model or slip-hardening behaviour or slip-softening behaviour. Some studies were done to understand the behaviour of FRC in practical situation. FRC was studied in the bridge deck cladding to enhance the ductility in case of earthquake or dynamic loads. They were even analyzed studies about thin FRC slabs or studies about the behaviour of FRC in case of blast. In the last years the research was focused on the behaviour of fibres with hooked-ends. This geometrical modification allow to improve all the smooth-end fibres' characteristics. Detailed FEM models were created able to describe a complete pull-out test. The creation of these complex FEM models was due to the hard analytical modelling of the hook straighten inside the matrix.
Even if there are a lot of papers and studies about FRC the experimentally data aren't fully available for all the range indicated in Table 1 or, are incomplete. Nevertheless

enough experimentally data are available, extrapolate from graph or papers tables, used to valid or void the different models.

1.3.1 Empirical models

In the literature of FRC, for empirical models, it means one or more equations used to describe a phenomena derived by experimental data fit. It means there is a first step where the experimental test is chosen and set with the purpose to better describe the looked behaviour. Secondly a "base function", it's a function that need to be calibrate with some parameters, is chosen. Usually this function is an exponential with few key-parameters. The final step is fit the experimental data with the base function chosen and modify the parameters until reach a satisfying fit. This type of model need a great sensibility and experience to choose the "base function", the mains parameters and the data to fit. In particular the last one is very important in FRC. Create empirical model to describe a complete pull-out or crack-bridging phenomena doesn't make sense. It doesn't make sense because the variability of materials and geometry is too large to have just one describing function. Indeed the use of empirical models in FRC is common with behaviour difficult to describe with mechanical relations. Empirical models are used to describe e.g. the location or orientation of the fibre as well as the effect of fibres inclination. In the hooked ends field empirical models are not really used due to the large number of variables. One example of empirical model in FRC with hooked-ends is in the modelling of the hook contribute using polynomial functions. The assumptions in other type of modelling make necessary the use of empirical model to describe some phenomena or to implement numerically.

modelling of proprieties and distribution of steel fibres within a fine aggregate concrete

With the purpose of studying the behaviour of cementitious composites containing different fine-grained mineral aggregates, a model to describe the fibre distribution and orientation was created. This model has fundamentals in statistics and there are two parameters, α and β, that adjust the formula for a good fit. A spatial function describes the α and β trends if the compound's characteristics change. Other data from the same specimens were fitted with exponential functions to describe the trend of main parameters such as volume fraction or Young's modulus.

Pull-out behaviour of steel fibers in self-compacting concrete

To study the influence of hooked ends in FRC an analytical model was developed. A first series of experiments with hooked ends and smooth fibres led to separating the hook influence. The possibility of this separation was even proved. Thereafter an analytical model to describe the smooth fibre debonding and pull-out stage was joined with an empirical model used to describe the hook contribution. To fit the experimental data of the hook contribution three polynomial functions were used, these simulate the hook contribution like an elastic spring. For the pull-out relation an energetic approach was used and two different friction relationships for the debonding and pull-out stage.

1.3.2 FEM models

A FEM model consist in mesh design of finite elements to reproduce a behaviour or phenomena. This type of modelling is quite appreciate because it give you all the parameters' value you wish that otherwise experimental test can't give just with one spaceman. The big obstacles are the creation of the model and the time for the solution. worth design a FEM model just if the information given to the calculator are quite complete and accurate. For this reason is usual to create a model just to recreate part of the overall phenomena. Even for time reason is important model phenomena with finite elements just if is strictly necessary or if the better understanding worth it. In FRC this type of modelling is often used to reproduce the matrix-fibre interface behaviour. Indeed interface finite elements are created ad hoc. The creation of new finite elements need fully understanding of the mathematical and physic relations used. To limit the time problem the symmetry of the fibre is used to reduce of one half the 3D mesh and 2D mesh. For straight fibres make sense create 2D model in order to use the symmetry of the problem and reduce problem linked to the numerical solution. In the hooked ends field a complete FEM simulation was done. It means that all the fibre, matrix and interface proprieties were keep in account with them non-linear behaviours. In this case a complex modelling, even if computationally heavy, make sense because allow to have data otherwise difficult to obtain.

Studies of the proprieties of the fiber-matrix interface in steel fiber reinforced mortar

A FEM analysis of the interface fibre-matrix behaviour is developed in this paper with the purpose of better understand the physical debond mechanism during the fibre pull-out,

and experimental data was used for its validation. Particular focus is on the adhesion coefficient determinate through the FEM model. The influence of polymer small fibres inside de mortar matrix (used to improve the interface bond) was even investigated and the results were compared with a simple mortar matrix in order to quantify the enhancement due to the polymer fibres. The experimental data presented in this paper was widely used to validate the Victor Li model and, the interface FEM model, was used as an example for the FEM modelling of the hook end.

Analysis of fiber debonding and pullout in composites

This paper describes an analytical model used to reproduce the debonding and pull-out stage in a single fibre pull-out test. An energetic approach, different from the more common mechanical one, is used to simulate the crack developed in the matrix-fibre interface. This approach considers the debonding zone as an interfacial crack that increases with an energetic criterion. A FEM model was made to reproduce the interface area during the debonding stage and calculate the mains energetic parameters. To validate the model it was compared with experimental tests.

Numerical modelling of the pull-out of hooked steel fibres from high strength cementitious matrix, supplemented by experimental results

A complete and refined FEM model of embedded fibre with hook end was studied, in particular this paper considers all the non-linearity present in the physical model even despite the simplicity and result timing thus applicability. Two different models were created (with 3D and 2D finite elements) and a comparison was made between them and experimental data. Furthermore the influence of different hook ends geometrical shape as well as different friction coefficients in the interface fibre-matrix was studied. The very refine FEM analysis, although computational heavy, allowed the understanding of the behaviour of an embedded fibre, indeed it was used often in the creation of the hook end straighten analytical model present in this thesis. It is also possible to use the data from the FEM model to validate or compare as well as the experimental data.

1.3.3 Analytical models

This type of modelling is based on mathematical and mechanical relations. Through some initial assumptions the mains mechanical relationships are written and put together to

create the final model. It means that the goodness of the model is quite influenced by the choice of the initials assumptions. A very detailed model is not useful because it need complicate mathematical functions difficult to implement. An equilibrium between simples functions and corrects assumptions is needed for a good analytical model. The FRC analytical models are mainly focus on the single fibre pull-out description. Nevertheless some of them describe the behaviour of composites with shorts fibres randomly distributed (crack-bridging models). Particular interest is in the matrix-fibre interface modelling during debonding stage as well as the fibre-matrix contact friction during the pull-out stage. Even for the fibres distribution and orientation some authors use a analytical-statistical approach to describe the probability density function. In the crack-bridging FRC models the overall model is made by 2 different equations those describe the debonding stage first and the pull-out stage next. In the modelling of hooked ends fibres is usual separate the slip behaviour and the hook straighten. The modelling of the hook straighten is quite difficult because it need big deformation theory, no-linear material and the section shape is not easy to integrate. It is even possible use a multi-linear analytical model to describe the whole pull-out behaviour, whereby any function has a displacement range of action.

Crack bridging in fiber reinforced cementitious composites with slip hardening interfaces

In this paper the pull-out model with slip-hardening developed by Victor Li is described. The analytical functions are first studied, describing the force-displacement relationship for a single fibre embedded in a cementitious matrix, subsequently the same functions are integrated with probability density distribution functions of fibre orientation and distribution to describe the behaviour of a complete composite. The analytical model is compared with experimental data (with polyethylene fibres). Furthermore, analysis of the composite ultimate stress and strain as well as the crack energy during the complete crack development is carried out. Probably the most important paper used in the thesis at issue, this paper was used to get the equation for the pull-out model, as for the single fibre pull-out force then for the composite with random fibres distribution and orientation, and to solve the probability density distribution functions and separate them from the rest of the integral.

Postcrack scaling relations for fiber reinforced cementitious composites

Victor Li's force-crack width simple analytical relationship is developed and compared with experimental data. The pull-out force of a single embedded fibre as well as the stress tension of a composite with random fibre distribution is analyzed with the assumption of a constant friction coefficient of the fibre-matrix interface. In this paper the fibre orientation influence through the snubbing factor and the crack energy in the cracking process of a FRC composite is studied. This is very useful for the comparison with the more detailed Victor Li model with slip hardening friction constitutive law.

Fiber debonding and pullout of elastic matrix

A debonding and pull-out analytical solution is analyzed in this paper. Different from the others models, here there are some assumptions that consider the poison coefficient and the concrete shrinkage. Usually they are neglected because numerically they are not really big and hard to explain with mathematical functions. Present in this paper is just a mechanical approach even for the matrix-fibre interface crack increasing. A weakness of this model is the necessity of an experimental calibration for a lot of coefficients. This treatise is made with a stress approach rather than with a displacement or force one.

Fiber pull out and bond slip .1: analytic study

Studied in this paper is a model used to describe a single straight fibre pull-out. A mechanical approach is used to describe the phenomena and particular focus is given to the fibre-matrix interface. In particular a bi-functional relationship describes the tension-displacement behaviour. After the complete fibre debond two types of function are used to describe the contact friction between fibre and matrix: one with constant trend and one with exponential softening branch. This is the first of two papers, the second one has the experimental validation of the model described in the first one.

A simple approach to model SFRC

The modelling of the pull-out behaviour starts from a micro scale model which afterwards is integrated into a macro scale model able to describe a crack bridging behaviour. All the main non-linearities are studied really well and keep in account the micro scale model, even orthotropic steel fibres were considered. Experimental tests are described and the data used to validate the model. Some tests were carried out on specimens taken from SFRC slag to study the influence of the boundary conditions in the fibre distribution and

orientation. With the results obtained a FEM model of a notched beam during bend test was created.

Modelling the pullout of hooked steel fibers from cementitious matrix

The purpose of this paper is to create a model to simulate the force-displacement relationship of hooked end steel fibres with a simple geometrical and mechanical analysis. The proposed model finds, with a few easy mechanical equations, the force needed to straighten the fibre's hook. Even the friction is considered through the coulomb's coefficient. Some important assumptions are made to use a simple approach but, nevertheless, the comparison with experimental data is satisfying. A good batch of data (with hook ends and without) allows a comparison also with other models or to validate the proposed model. This is very useful because it uses a simple approach, and is thus usable in a numerical implementation, compared to a very complicated one. This paper was used to compare the model and for the experimental data as well.

Predicting the pull-out response of inclined hooked steel fibres

In this paper the analytical model used to describe the pull-out behaviour considers even the fibre orientation. Initially a pull-out test was done to subdivide the behaviour in different branches. Subsequently every single part was analyzed separately and models using mechanical relations were created. Finally they are joined together for the overall model. The analysis of the fibre orientation is quite good, indeed it keeps in account the cementitious matrix spalling as well.

Chapter 2

Constitutive model

The numerical solution needs a study about an analytic model and all the hypothesis and simplifications adopted. In the first part of this chapter the analytical model used is described and the motivation that lead us to its assumption, latter the numerical model used for the solution implementation.

2.1 crack bridging analytical model

The basic numerical model adopted to describe the pull-out model is based on the work of Lin and Li[1]. The reasons that lead to the choice of this model are:

- simple use of the model
- availability of a complete analytic solution
- good fit with experimentally data

A summary of several others models from different authors was presented in Chapter 1 but for the reasons stated above the model of Lin and Li [1] was selected.

This model is subdivided in more steps. Firstly the pull-out of a single straight fibre with the load force aligned with its axis is considered, secondary, the possibility of an inclined fibre with orientation angle "ϕ" (angle formed by the fibre with the orthogonal matrix crack plane considered uniformly plan) and, finally, the crack-bridging model with a probability distribution of fibres distribution, embedded length fibres and angle orientation (3-D). Step by step the model is more refined and complete nevertheless with the introduction of simplifying assumptions.

2.1.1 Main initial hypothesis

The analytic solution for the fibre pull-out is based on some initial hypothesis [6], necessary to render easy and controllable the mathematic relationship:

- the matrix crack is planar
- the matrix deformation is negligible during fibre pull-out
- the fibres have 3-D random distribution in location and orientation
- the fibres are straight with cylindrical geometry
- the fibres behave linear elastically

- the Poisson effect of the fibre on pull-out is neglected
- thermal dilatation and concrete shrinkage are neglected
- the fibre-matrix bond is frictional with slip-hardening
- elastic bond strength is neglected

The first hypothesis regard the geometry of the fibre because the radial dimension is very small so a little no-planar crack effect is negligible and the probability of a big no-planar crack is low. For the weak shear elastic stress of the cementitious composites and for the negligible energy absorption the matrix elastic deformation before the debonding is considered null. About Poisson effect, thermal dilatation and concrete shrinkage, neglected in this model, are done relevant hypothesis because in others mathematical model [5] are keep in account but for the low stress present in a single fibre and the Young module of the steel (this treatise is focus mainly on that material) consent to not consider it. Furthermore the last 2 physic effects should be considerate just in particular situation and geometry. The slip-hardening behaviour and the elastic bond strength are the representative elements of this model how will explain after.

2.1.2 Interface constitutive relationship

To describe the relationship between matrix and fibre contact's surface, the following constitutive law has been used:

$$\tau = \tau(S) \tag{2.1}$$

where:

τ = interface shear stress

S = fibre slip

This equation draws attention to the only one variable dependence and to the fact that the linear elastic bond is neglected. Indeed, the variable, consider just a contact frictional relation.

The linear slip hardening constitutive law given in equation 2.2 and illustrated in (Fig.2.1) was assumed.

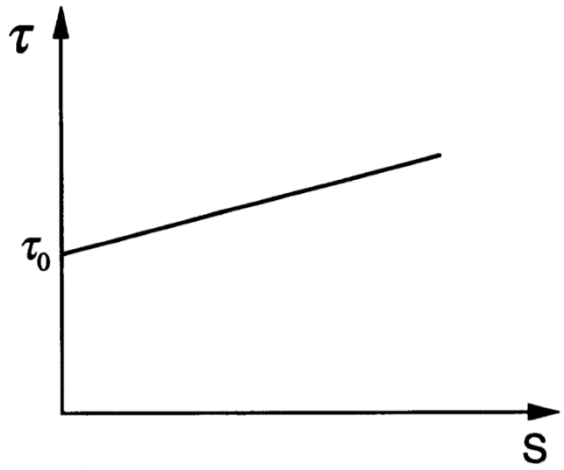

Fig. 2.1 *Linear slip hardening relationship*

$$\tau = \tau_0 \cdot (1 + \beta \cdot S/d_f) \qquad (2.2)$$

where:

τ_0 = frictional sliding shear stress at the tip of debonding zone

β = non-dimensional hardening parameter

d_f = diameter of the fibre

The formula shows that the interface constitutive relationship depends upon the geometry of the fibre (via d_f) and also upon fibre-matrix interface parameters β and τ_0 that need to be determined empirically.

2.1.3 Single fibre pull-out

Next, Lin and Li considered the relationship between the applied load to a single straight fibre and its slipping respect the matrix (for hypothesis considered endeformable), after local equilibrium and congruent equations [1] the below relations are obtained

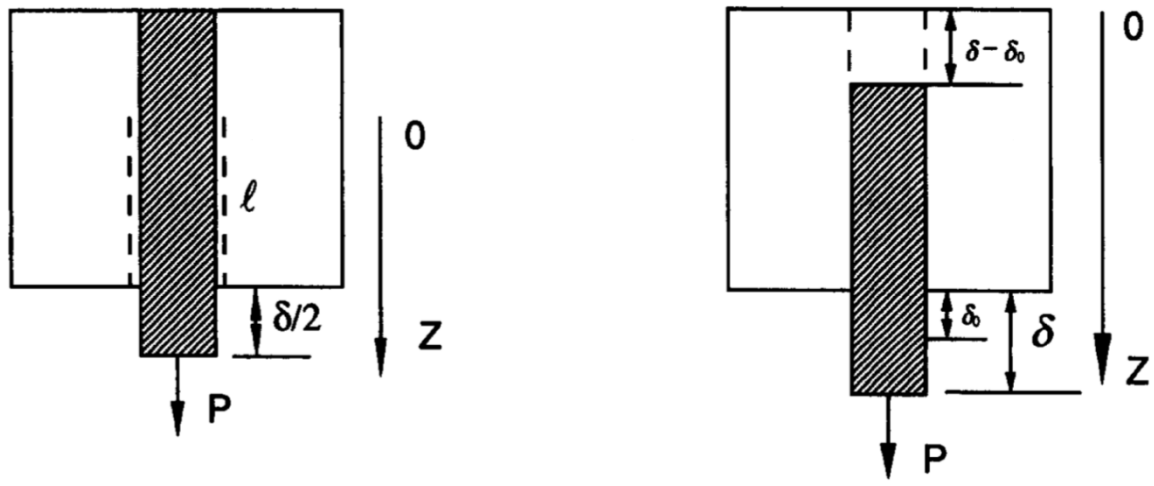

(a) *(b)*

Fig 2.2 *Geometrical meaning of pre-debonding slip (a) and post-debonding slip (b), "ℓ" is the debond/slide region(when the fibre is completely debond his value is equal to L)*

$$P = \frac{\pi d_f \tau_0 (1+\eta)}{\omega} \sqrt{\left(1 + \frac{\beta\delta}{2d_f}\right)^2 - 1} \tag{2.3}$$

For $0 \le \delta \le \delta_0$

$$P = \frac{\pi {d_f}^2 \tau_0 (1+\eta)}{\omega} \left[\sinh\left(\frac{\omega L}{d_f}\right) + \sinh\left(\frac{\omega(\delta-\delta_0)}{d_f}\right)\right] + \pi\tau_0\beta(1+\eta)(\delta-\delta_0)\left(L-(\delta-\delta_0)\right) \tag{2.4}$$

For $\delta_0 \le \delta \le L$

$$\eta = \frac{V_f E_f}{V_m E_m} \tag{2.5}$$

$$\omega = \sqrt{4(1+\eta)\,\beta\tau_0/E_f} \tag{2.6}$$

$$\delta_0 = \frac{2d_f}{\beta}\left[\cosh\left(\frac{\omega L}{d_f}\right) - 1\right] \tag{2.7}$$

L = embedded fibre length

$$P = 0 \tag{2.8}$$

For $L < \delta$

As is possible see from the relations above the pull-out load "P(δ)" depends upon geometrical parameters V_f, d_f, L_f and mechanical parameters β and τ_0. These parameters identify the characteristics of the fibre, whereas the matrix propriety are define with just one parameter E_m. The validity of these formulas depends by a correct adjustment of the mechanical parameters β and τ_0, this calibration may be done fitting experimentally data regarding the type of fibre and matrix are considered.

2.1.3.1 Snubbing coefficient

The treatise until this point consider the load force "P" aligned with the fibre axis, hence to keep in account the eventual inclination of the fibre with angle φ is simply necessary multiply the straight fibre pull-out force for a term that consider the inclination of the fibre:

$$P(\delta, \Phi) = P(\delta, \Phi = 0) \cdot e^{f\Phi} \tag{2.9}$$

f = snubbing coefficient

the value of the snubbing coefficient can be determined experimentally and its range is 0.7 - 0.9 for a angle up to 80° [1].
The mathematical simplicity of this relation consent to easily solve the relative integral and to focus the effect of the angle just in one, continues and derivable function "$e^{f\Phi}$".

2.1.4 Probability density functions

To consider a casual insert of fibres in a concrete matrix, so without control about fibres distribution, location and orientation, was done a statistical study about fibres orientation, spatial distribution and quantity of broken fibres [6]. These 3 different studies are

completely independent between them if not for the initial assumptions. Variables nomenclature is shown below for a single embedded fibre (Fig. 2.3).

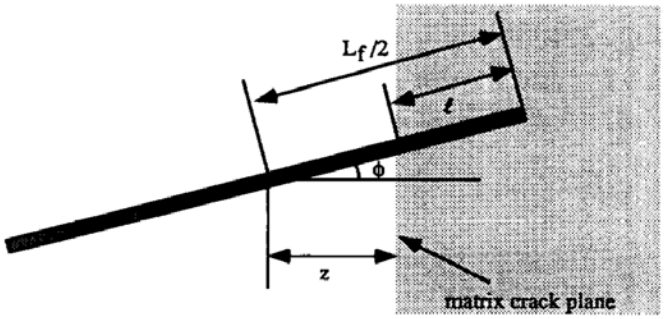

Fig. 2.3 *Single fibre embedded in a cementitious matrix*

2.1.4.1 Orientation angle

As written above, the probability function, consider a spatial (3D) distribution of a single fibre embedded.

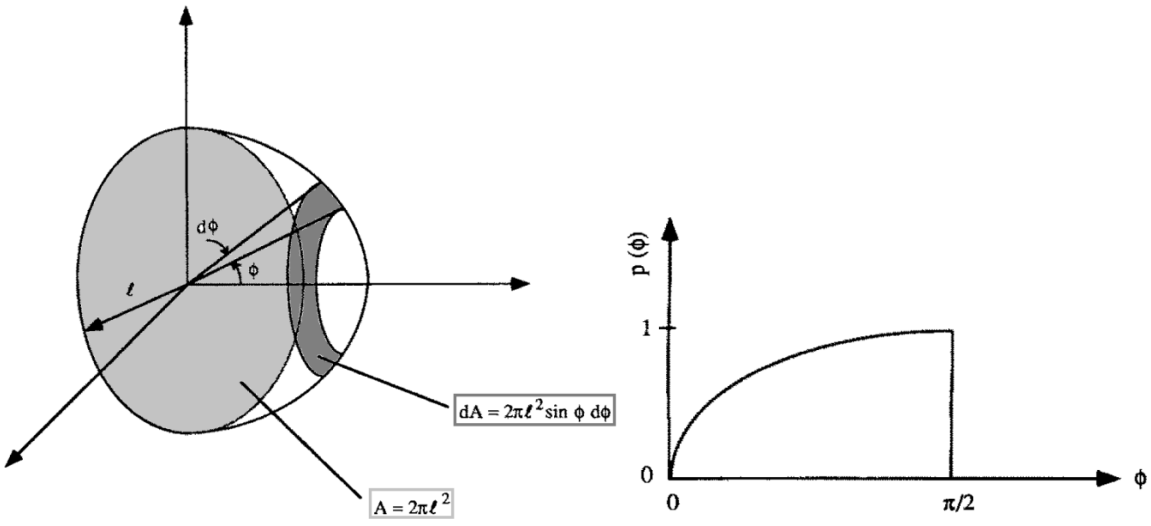

(a) *(b)*

Fig. 2.4 *3D spatial distribution (a), probability density function p(Φ) (b)*

By the mathematical definition we have [6]:

$$p(\Phi) = \frac{1}{A} \cdot \frac{dA}{d\emptyset} = \sin \emptyset \qquad (2.10)$$

For $0 \leq \Phi \leq \pi/2$

The hypothesis of planar crack of the cementitius matrix allow to use just a parameter to consider a 3D distribution, obviously the range is 0 - $\pi/2$ because for angles bigger then $\pi/2$ is possible consider the other half part of the fibre (practical explanation).

2.1.4.2 Spatial distribution

Probability density function considers fibre spread with a uniform distribution onto the entire crack surface.

$$p(z) = \frac{L_f}{2} \tag{2.11}$$

For $0 \leq z \leq L_f/2$

The meaning of the p(z) is to consider the presence of a fibre up to half fibre distance, hence it keep in account a distribution easier and more regular possible.

2.1.4.3 Embedded length fibres

Experimentally studies demonstrate the presence of fibres don't embedded for the whole length, that invalid or reduce them contribute to the compound resistance, to keep in account this fact is introduced a coefficient "a_{ef}". This coefficient reduces the number of fibre determinate with the volume fraction (V_f). For simplicity a_{ef} is a linear coefficient so may be applied at every step of the analysis and $0 \leq a_{ef} \leq 1$ where if $a_{ef} = 1$ means that the contribute of the all length of the fibres is considered.

2.1.5 Model equations

To get the solution for a composite with randomly distributed discontinues fibres of volume fraction V_f is necessary solve the integral below [1]

$$\sigma_B(\delta) = \frac{4 \cdot V_f}{\pi \cdot d_f^2} \cdot \int_{\emptyset=0}^{\pi/2} \int_{z=0}^{(L_f/2)\cdot \cos \emptyset} P(\delta) \cdot p(\emptyset) \cdot p(z) dz d\emptyset \tag{2.12a}$$

And after rather tedious derivation and simplifying assumptions, the final equations are:

$$\frac{\sigma_B}{\sigma_0} = \begin{cases} \frac{2}{k}\left\{\left[1 - \frac{1}{k}\cosh^{-1}\left(1 + \lambda\frac{\delta}{\delta^*}\right)\right]\sqrt{\left(1 + \lambda\frac{\delta}{\delta^*}\right)^2 - 1} + \frac{\lambda}{k}\frac{\delta}{\delta^*}\right\} & (0 \le \bar{\delta} \le \bar{\delta}^*) \\ \left(1 + \frac{\beta L_f}{2d_f}\delta\right)(1 - \delta) & (\bar{\delta}^* \le \bar{\delta} \le 1) \\ 0 & (\bar{\delta} \ge 1) \end{cases}$$

(2.12/13/14)

where:

$$\sigma_0 = \frac{1}{2} g \tau_0 V_f (1 + \eta) L_f / d_f \quad (2.15)$$

$$k = \omega L_f/(2d_f) \quad (2.16)$$

$$\lambda = \cosh(k) - 1 \quad (2.17)$$

$$\bar{\delta} = \delta/(L_f/2) \quad (2.18)$$

$$\bar{\delta^*} = \frac{2d_f}{\beta}[\cosh(k) - 1]/(L_f/2) \quad (2.19)$$

$$g = \frac{2}{4+f^2}(1 + e^{f\pi/2}) \quad (2.20)$$

$$\eta = \frac{V_f E_f}{V_m E_m} \quad (2.21)$$

$$\omega = \sqrt{\frac{4(1+\eta)\beta\tau_0}{E_f}} \quad (2.22)$$

The final solution is subdivided in 3 equations where:

- (2.13) consider the pre-debonding stage, where part of the embedded portion of the fibre is still bridging to the matrix.
- (2.14) give the solution for the post-debonding stage, thus when the fibre is completely debond and the interface force is given by the frictional linear-hardening model.
- (2.15) evidence the annulment of the contribution of the fibre when it is completely out from the matrix.

In derivation of the first equation has been considerate [6] the different behaviour of the part of the fibres debond and the part of fibre not yet debond. In the relation above particular importance is given by (2.20) because it represents the fibre orientation probability density.

2.2 Pull-out numerical model

For the implementation of the Victor Li equations [6] is used the calculate code “Mathcad 15” because simple to use and enough powerfully and quick for the level of the analysis needed at the moment. The main program is subdivided mainly in three step:

1. Data input: this part consist in some line of code where is possible insert the characteristics of the matrix, of the fibres and the others parameters about the interface matrix-fibre bond. In this step are included the parameters regard the Victor Li treatise [1] (e.g. Snubbing factor, σ_0 and others), as you can see in the figure below (Fig.2.5), this parameters consider a “sin(ϕ)” probability density distribution of the fibres orientation angles and a snubbing coefficient f=0.6 (as suggest in [1]).

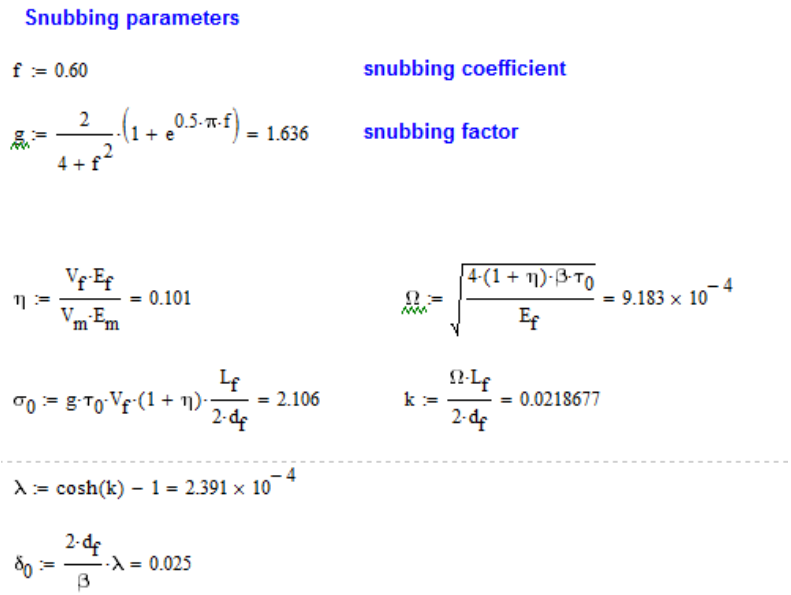

Fig. 2.5 *Line of the main program relative to the Victor Li parameters*

2. Matrix crack model: in this part there is the hug of the program with the calculation of crack width, stress tension and compound damage. The crack model used in this was taken from [7] and it isn’t particularly described because is not the purpose of this study.
3. Data output: this ending part include the experimentally data [8] for the comparison and the graphic part with charts, both used to calibrate the model parameters with the purpose to obtain the best fit possible (Fig. 2.6)

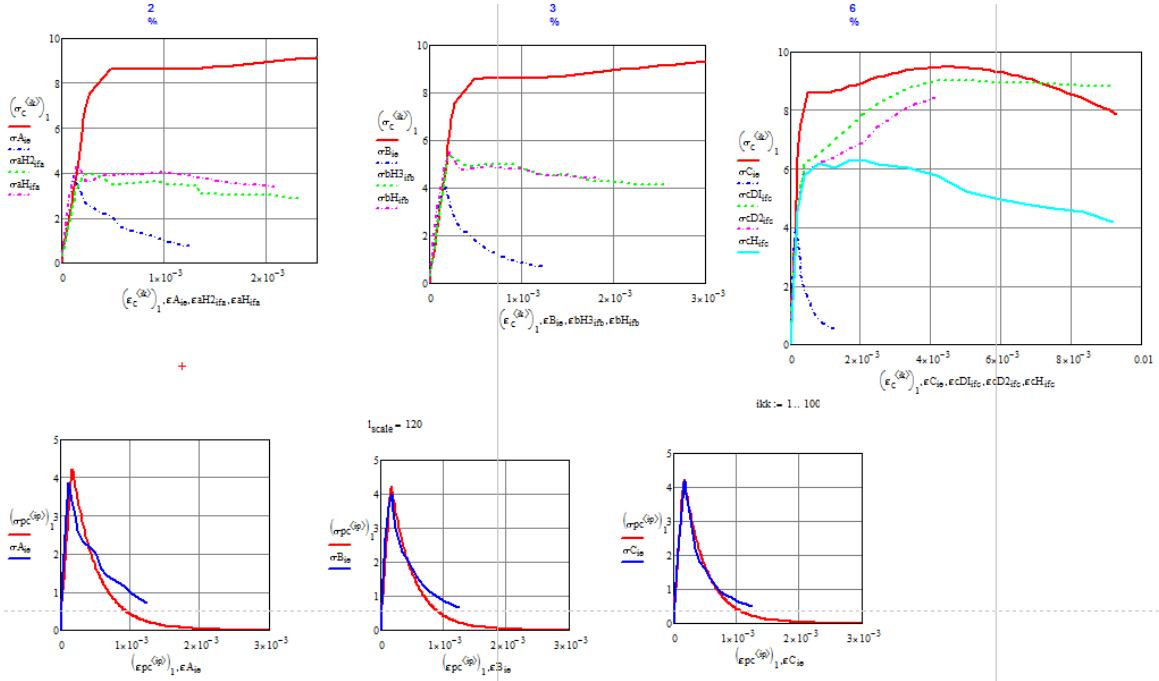

Fig. 2.6 *Graphic output for the calibration of the parameters*

The original model above described was subsequently modified to obtain a model that describe as better as possible the behaviour of the FRC. Nevertheless, for some simple analysis, was used a simplified model because easier to use, modify and, mainly, to control.

Chapter 3

Analysis of the pull-out model

To improve and better understand the model previously described were done some studies and analysis about the interface matrix-fibre and likelihood's distribution regard the fibres location, the results and feedbacks obtain are below written

3.1 Influence of the pull-out model parameters

The influence of the main model parameters on the predicted force-displacement response given by crack bridging model of Lin and Li [1] was investigated in a parametric study.

3.1.1 Analysis setting

For this study, it was necessary to identify the mains parameters and the meaningful ranges for the analysis. This information is based on the recommendations given by Lin and Li [1] as well as on observations from experimental pull-out tests [1,12] and is summarised in table 3.1.

Table 3.1 *Analysis data range and information*

	Parameters	**Measurement unit**	**Range**
INPUT PARAMETERS	V_f	%	0.5 - 2 - 3.5 - 5 - 6
	L_f/d_f	/	25 - 45 - 65 - 85 - 100
	β	/	0.01 - 0.015 - 0.03 - 0.045 - 0.05 - 0.1 - 0.2 - 0.3 - 0.5
	τ_0	MPa	0.5 - 1 - 1.5 - 2 - 3
	Parameter	**Measurement unit**	**Description**
OUTPUT PARAMETERS	Max δd	mm	Maximum displacement of the fibre during the debonding stage
	σ_{db}	MPa	Complete debonding tension
	Max δv	mm	Maximum displacement of the fibre
	σ_{po}	MPa	Maximum crack-bridging stress

The values in table 3.1 cover a wide but meaningful range and refer to the fibres proprieties. The range of β is wider than the others because, for different type of fibres it can have significantly different values, with a possible change of magnitude, depending on the type of fibre material (i.e. polyethylene or steel), and this model is not just for a specific fibre's material. Normalized stresses were used to compare the results and these were obtained by dividing the crack-bridging stress by σ_0.

The Mathcad code used to obtain the results is given below and consists of the constitutive pull-out equations of the model (Fig. 3.1). A a simple displacement subdividing algorithm (Fig. 3.2) is used to obtain the σ-δ relationship trend with regular displacement steps; smaller for the debonding stage than for the pull-out stage (Fig. 3.3).

Crack bridging relationship:

$$\sigma_B(\delta) := \begin{| \sigma b \leftarrow \sigma_0 \cdot \frac{2}{k} \cdot \left[\left(1 - \frac{1}{k} \cdot \operatorname{acosh}\left(1 + \lambda \cdot \frac{\delta}{\delta_0} \right) \right) \cdot \sqrt{\left(1 + \lambda \cdot \frac{\delta}{\delta_0} \right)^2 - 1} + \frac{\lambda}{k} \cdot \frac{\delta}{\delta_0} \right] \text{ if } \delta \geq 0 \wedge \delta \leq \delta_0 \\ \sigma b \leftarrow \sigma_0 \cdot \left(1 + \frac{\beta}{d_f} \cdot \delta \right) \cdot \left(1 - \frac{2 \cdot \delta}{L_f} \right)^2 \text{ if } \delta > \delta_0 \wedge \delta \leq \frac{L_f}{2} \\ \sigma b \leftarrow 0 \text{ if } \delta > \frac{L_f}{2} \\ \sigma b \end|$$

Fig. 3.1 *code lines regard the σ-δ relationship*

$nstep := 100$

$i := 1 .. nstep$

$$\delta v_i := \frac{i - 1}{nstep - 1} \cdot \frac{L_f}{2} \qquad \delta d_i := \frac{i - 1}{nstep - 1} \cdot \delta_0 \cdot 1.0$$

$$\begin{| \text{for } i \in 1 .. nstep \\ \quad \delta v_i \leftarrow \frac{i - 1}{nstep - 1} \cdot \frac{L_f}{2} \\ \quad \delta d_i \leftarrow \frac{i - 1}{nstep - 1} \cdot \delta_0 \cdot 1.0 \\ \quad \text{trace}\left("\delta v \{0\} \delta d \{1\} " , \delta v_i , \delta d_i \right) \\ \delta v_i \end|$$

Fig. 3.2 *Displacement steps algorithm*

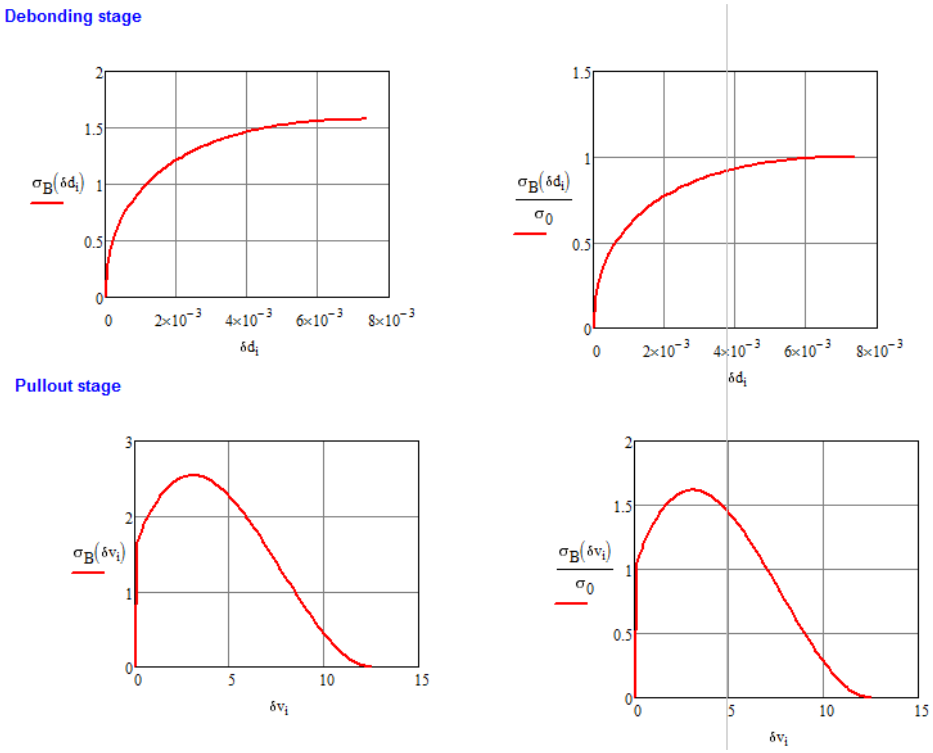

Fig. 3.3 *Output charts for the debonding and pull-out stage (are included the zero-dimensional charts)*

As the equation shown, the model response depends upon several parameters simultaneously. Thus, during the study of one parameter, average value for the others fibre parameters were employed. The assumption of average values for the others parameters is acceptable because the interest of this analysis is in the trend of the output and not in the numerical value and the trend is independent from the others parameters.

3.1.2 Output remarks

Although the results obtain in this parametric study are not directly applicable for any application, they are very useful in understanding the behaviour of the FRC and to better control and calibrate the model parameters for the subsequently analysis.

3.1.2.1 Volume fraction analysis

For the analysis of the volume fraction the average value of the others parameters of the fibres are $L_f/d_f = 50$, $\beta = 0.03$ and $\tau_0 = 2$ MPa.

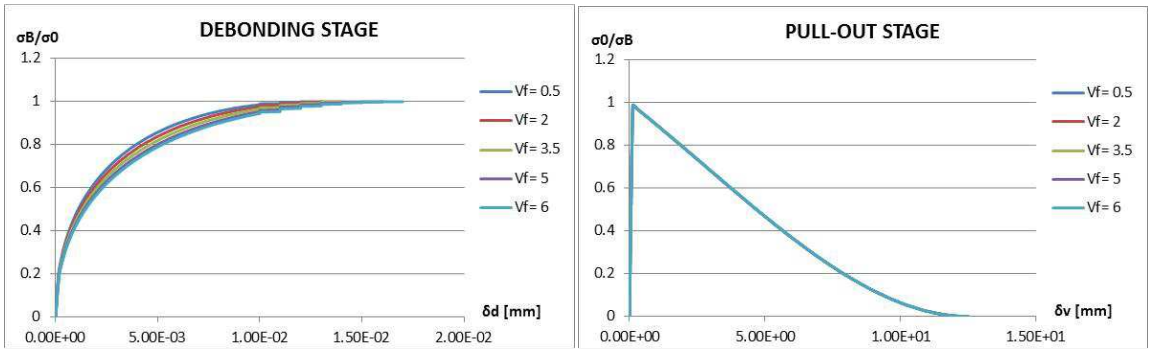

Fig. 3.4 *Variation of the behaviour during (a) the debonding stage and (b) the pull-out stage*

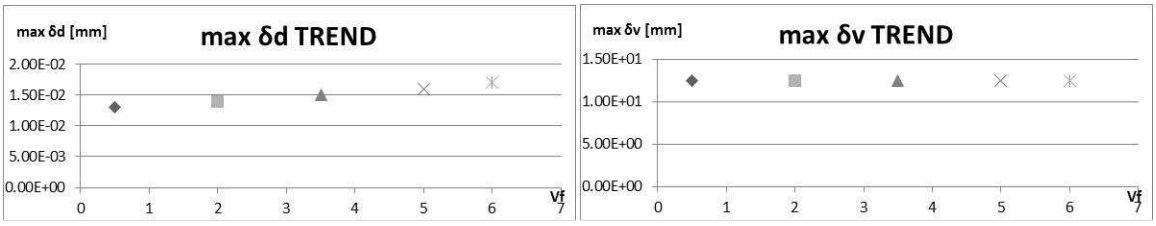

Fig. 3.4 *Displacement trend during (c) debonding stage and (d) pull-out stage*

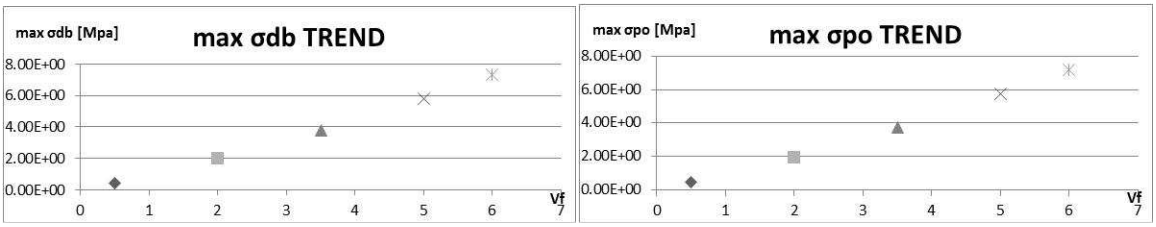

Fig. 3.4 *Stress trend during (e) debonding stage and (f) pull-out stage*

With the increase of the volume fraction only the behaviour of the debonding stage changes with a weak increment of the initial stiffness but the maximum zero-dimensional value of stress doesn't change (Fig. 3.4a). This fact is due to the parallel increase of σ_0, indeed V_f has a great effect on σ_0. An apparently linear relationship between the maximum debonding displacement and V_f and between stress and V_f is observed (Fig. 3.4c,e).

3.1.2.2 Aspect ratio analysis

For the analysis of the fibres aspect ratio the average value of the others model parameters are V_f = 3%, β = 0.03 and τ_0 = 2 MPa.

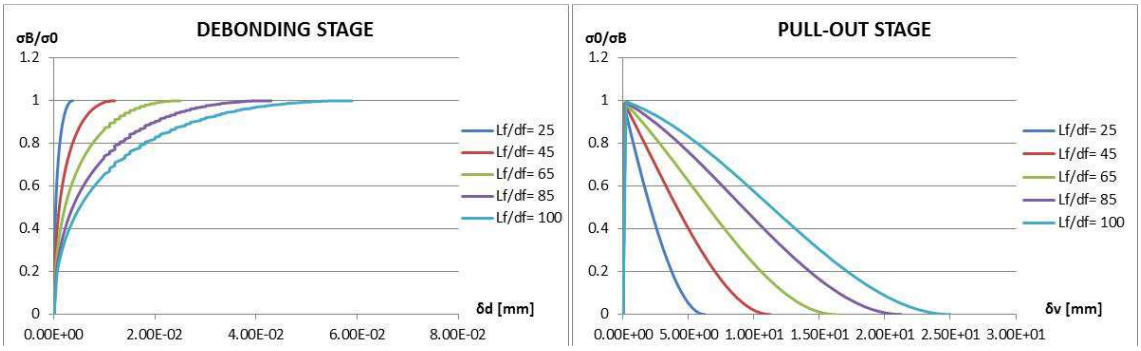

Fig. 3.5 *Variation of the behaviour during (a) the debonding stage and (b) the pull-out stage*

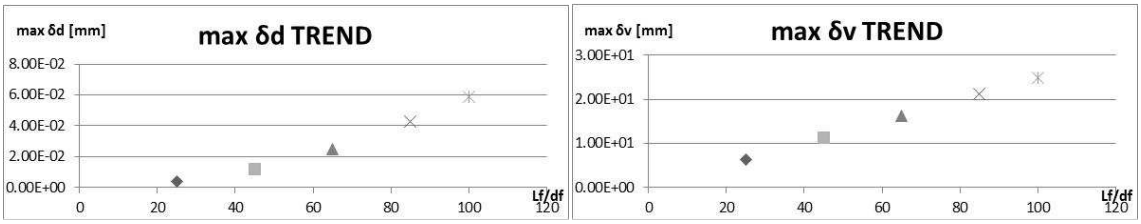

Fig. 3.5 *Displacement trend during (c) debonding stage and (d) pull-out stage*

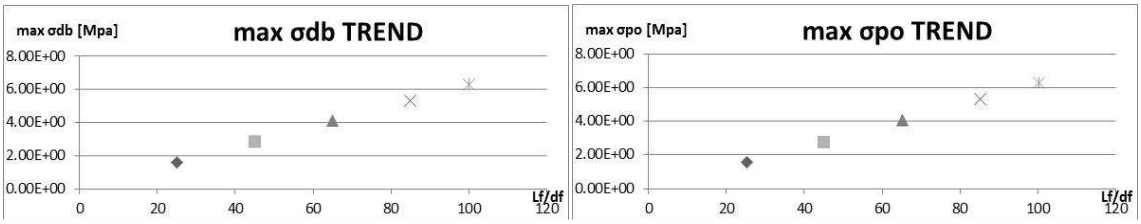

Fig. 3.5 *Stress trend during (e) debonding stage and (f) pull-out stage*

The increase of the aspect ratio results in a loss of stiffness in the debonding stage with consequent increase of the last displacement before reach the complete debond (Fig. 3.5a). that increase has a apparently not-linear trend (Fig. 3.5c), but, the effects of the aspect ratio are also evident in the pull-out stage with a linear relationship that link the increase of the last displacement and the maximum stress (Fig. 3.5d,e,f).

3.1.2.3 Beta analysis

For the analysis of the non-dimensional hardening parameter β, the average value of the others model parameters are V_f = 3%, L_f/d_f = 50 and τ_0 = 2 MPa.

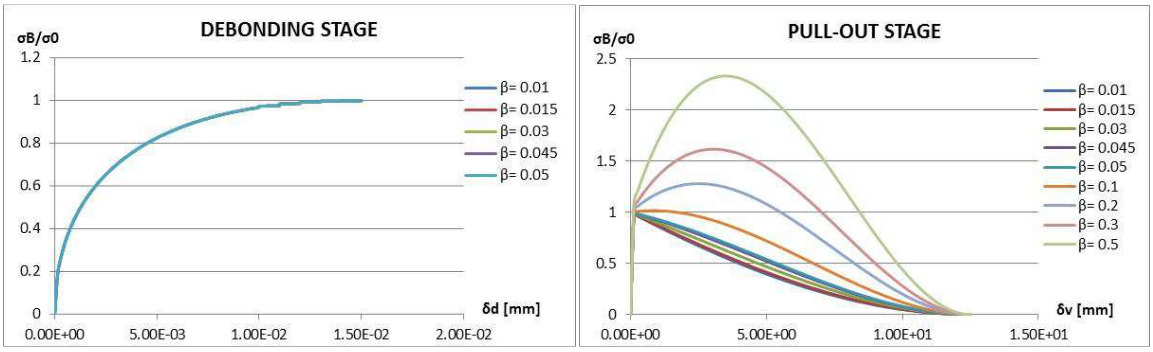

Fig. 3.6 *Variation of the behaviour during (a) the debonding stage and (b) the pull-out stage*

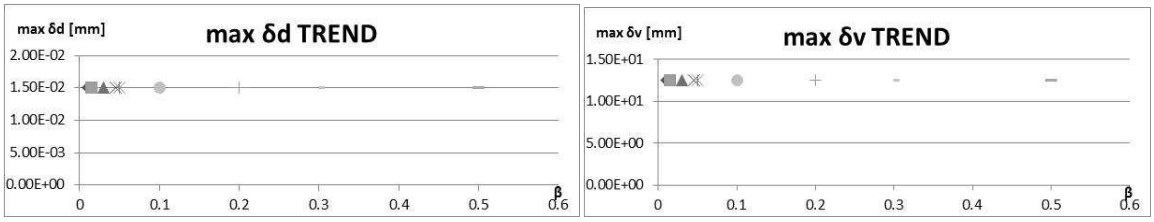

Fig. 3.6 *Displacement trend during (c) debonding stage and (d) pull-out stage*

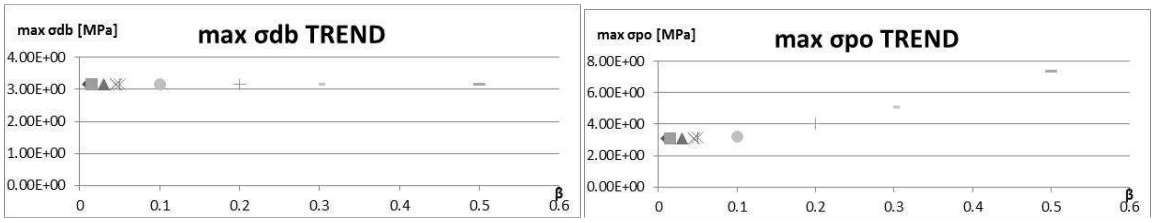

Fig. 3.6 *Stress trend during (e) debonding stage and (f) pull-out stage*

The influence of β on the predicted response is evident only in the pull-out stage, as can be seen in Fig (3.6a,b). This is because β characterizes the slip-hardening behaviour and the slip in the debonding stage is negligible but not neglected (Fig. 3.6a). For small values of β the improvement of ductility is weak but, for values higher than 0.1, the pull-out stage show a large area underlying that means that the energy dissipated during fibre pull-out stage increases considerably. The increase of the maximum stress for high values of β is evident and non-linear (Fig. 3.6f).

3.1.2.4 Sliding shear stress analysis

For the analysis of the τ_0 tension stress the average value of the others model parameters are V_f = 3%, L_f/d_f = 50 and β = 0.03.

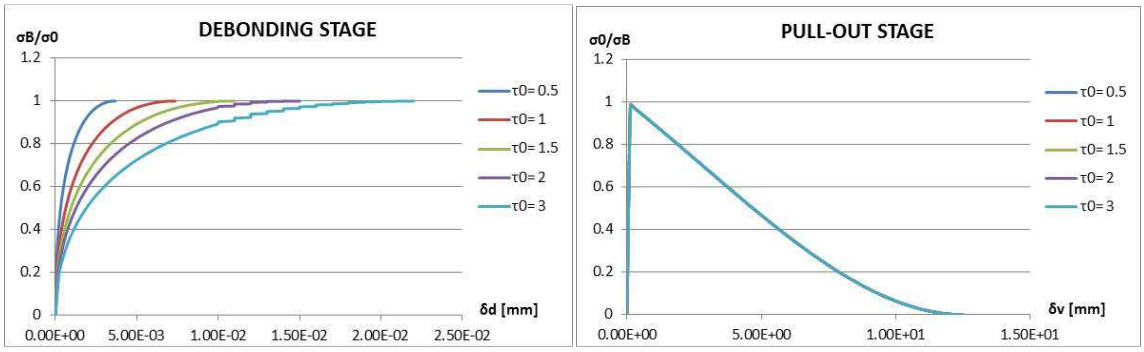

Fig. 3.7 *Variation of the behaviour during (a) the debonding stage and (b) the pull-out*

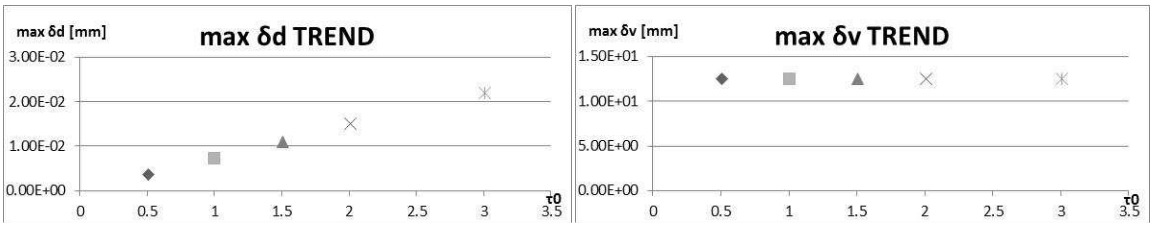

Fig. 3.7 *Displacement trend during (c) debonding stage and (d) pull-out stage*

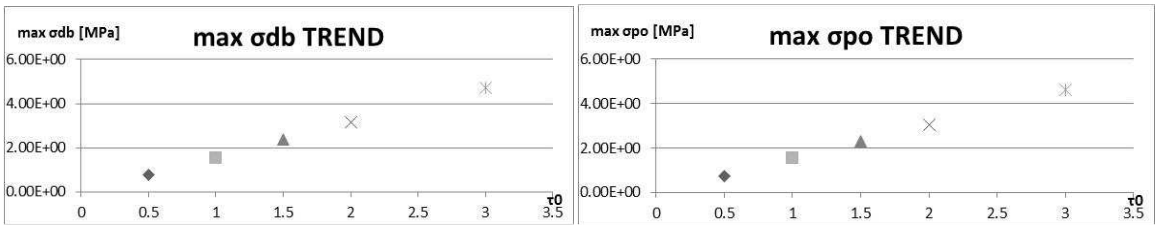

Fig. 3.7 *Stress trend during (e) debonding stage and (f) pull-out stage*

The effect of τ_0 interest just the debonding stage when the slip is small (Fig. 3.7a,b) and whereby the main contribute is got by the constant value of the matrix-fibre interface function than by the parameters that depend by the slip. With the increase of its value displacement and stress have a linear increment trend (Fig. 3.7c) whereas the pull-out stage parameters values remain constant (Fig. 3.7d).

3.2 Setting and validation of the model

This study is focused on the behaviour of steel fibres (nevertheless the model could be used for others fibre materials) and the aim is to understand values and range of values that are meaningful for steel fibres. For this purpose, numerical simulations were run n which the main parameters β, τ_0 and a_{ef} were changed until the best possible fit of experimental data from tensile tests on steel fibre reinforced specimens [8] was found. Once find the best fit possible was found, the same analysis with the τ-constant [13] model was carried out to validate or overrule the hypothesis of slip-hardening behaviour.

3.2.1 Setting analysis

Numerical simulations were run with the main model (implemented in Mathcad) in order to find the set of parameters that would best characterize the experimental results given in [8]. These values are obtained with a displacement-control test in order to describe the whole behaviour during the fibre debonding and pull-out stages. The data refers to one type of steel fibres embedded in 3 different concrete matrices with the characteristics shown below in table 3.2.

Table 3.2 *Test analysis characteristics*

Fibres characteristic	**name**	**L_f [mm]**	**d_f [mm]**	**L_f/d_f**	**E_f [MPa]**
	HAREX	32	0.8	40	200000

Specimen characteristic	**name**	**Fibre type**	**Matrix**	**E_c [MPa]**	**F_{tm} [MPa]**	**u_0 [mm]**	**V_f [%]**
	A111	HAREX	A	30000	3.65	0.45	2
	A112	HAREX	A	30000	3.65	0.45	2
	B211	HAREX	B	28000	3.62	0.49	3
	B212	HAREX	B	28000	3.62	0.49	3
	C311	HAREX	C	20000	3.24	0.34	6

Model characteristic	**l_{scale} [mm]**	**Snubbing coefficient**	**p(ϕ)**
	120	0.6	sin(ϕ)

The differences between the matrices depend mainly on W/C ratio and aggregate/binder ratio. 5 different types of data were fit with the results shown in the charts below.

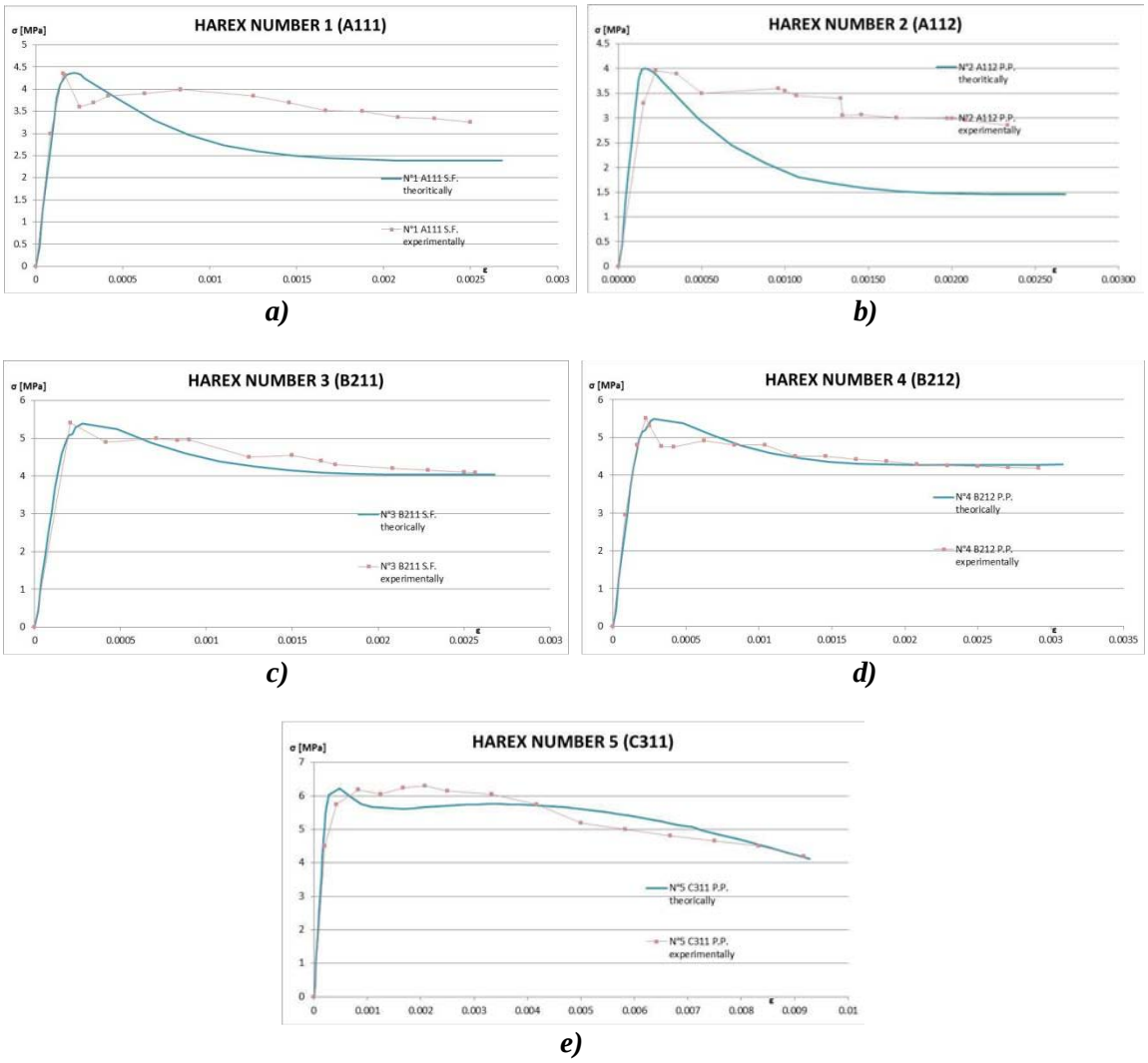

Fig. 3.8 *Model response with ideal parameters*

The graphs presented above show that the best fit is obtained for higher fibre volume fractions (Fig. 3.8 d,e). It is also observed the trend of the experimentally data is not exactly the same as the theoretically one. Indeed for the same set of experiments the results can be different. It is due i.e. to the concrete non homogeneous or human errors. Nevertheless the assumptions used for the model are simplification of the real behaviour, therefore they make errors. Furthermore the mathematical description of random fibres distribution is still quite difficult. However, the predict pull-out response describes in a satisfying level the behaviour observed in experiments. The effect of using different matrix proprieties are weak; the characteristic of the concrete matrix have an influence only on the first branch, before the matrix starts to crack. Indeed, the fitting in that branch is excellent. There is no any apparent correlation between the volume fraction (Fig. 3.9) and the main proprieties of the fibres. For higher fibre volume fractions (6%) the values

have an apparent shift from the others, but, the information available is insufficient to confirm or explain this shift.

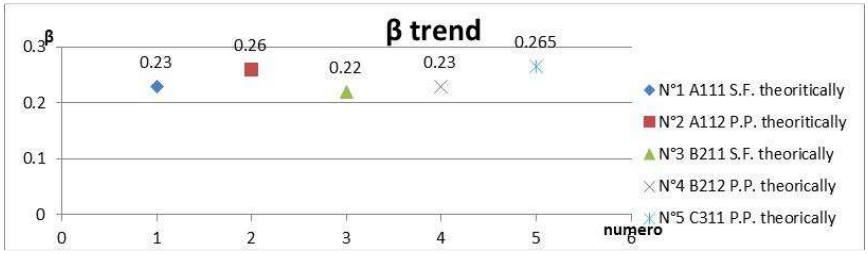

a)

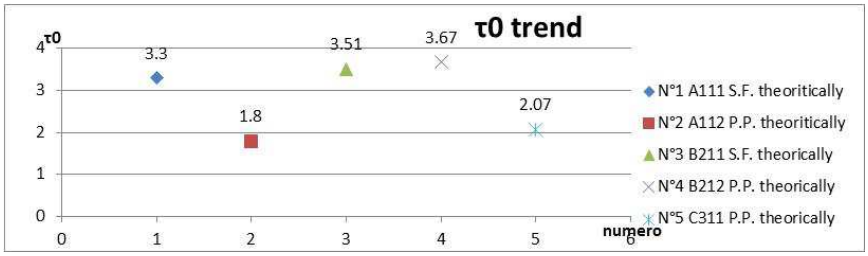

b)

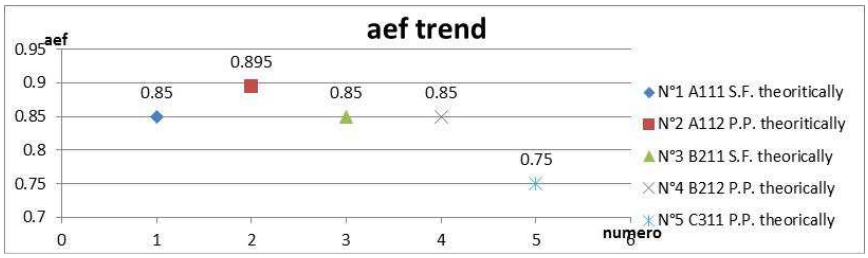

c)

***Fig. 3.9** Main fibres' parameters trend*

This analysis makes it possible to assess and obtain the representative ranges and average values for the steel fibre and fibre-matrix proprieties that are employed in the model. These are given in table 3.3.

***Table 3.3** Main parameters setting values*

Parameter	Range	Average	Comments
β	0.22 – 0.265	0.241	This parameter remains quite stable around the value of 2.3 nevertheless the slope of the hardening branch is completely different if the V_f change.
τ_0	1.8 – 3.67	2.87	It is evident the decrease of τ_0 in 2 cases but, it isn't link to the different value of V_f. Also if the average value is less than 3 MPa most of the results are around 3.4 MPa.

a_{ef}	0.75 – 0.895	0.839	Even in this case several values shift from the average value, mainly, the V_f = 6% value's shift could be caused by the interference of the binder surface or by the casting direction. The value of 0.8 for this coefficient was found [14] through some experiments.

3.2.2 Validation of the slip-hardening behaviour

To confirm the hypothesis of hardening behaviour in the interface shear stress-slip relationship, a comparison with the τ_0-constant model was carried out. To get the best fit, different values of the fibres parameters was used for the τ_0-constant model (Fig. 3.10). The set of parameters in this model obviously exclude β, which is a hardening parameter. Because β influences the response in the debonding stage as well as in the pull-out stage, it is not surprising that the τ_0-constant model requires higher values for the main parameters than the slip-hardening pull-out model.

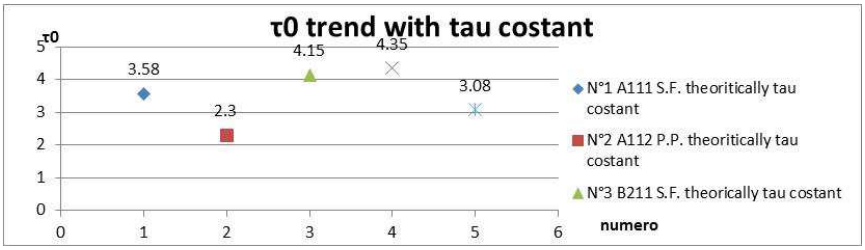

a)

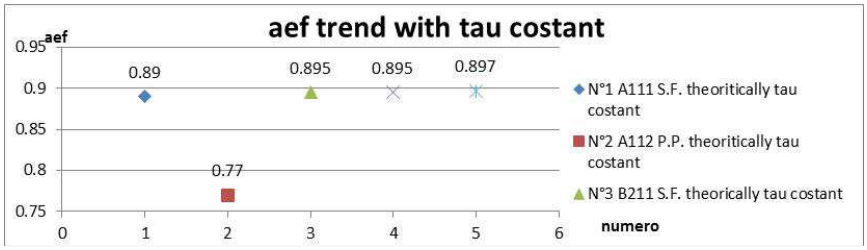

b)

Fig. 3.10 *Main fibres' parameters trend with τ_0-constant*

The graphs show a constant increase of 0.8 MPa in the τ_0 parameter, compared to the values required when using the slip hardening model, for all the specimens (Fig. 3.10a). These results allow us to assess the influence of the hardening parameter β by comparison between the two different models. A rise of the values of a_{ef} parameter is also observed (Fig. 3.10b). This is believed to be due to the fact that high fibres length using is

necessary to enhance the material response. In this model there are some parameters that shift from the average values estimable in Fig 3.10 but nevertheless are not sufficient to invalidate the test or the τ_0-constant model. The comparison of the slip-hardening model with τ_0-constant model justifies the effort done to solve and implement the more complex equations used by the first one to describe the FRC behaviour.

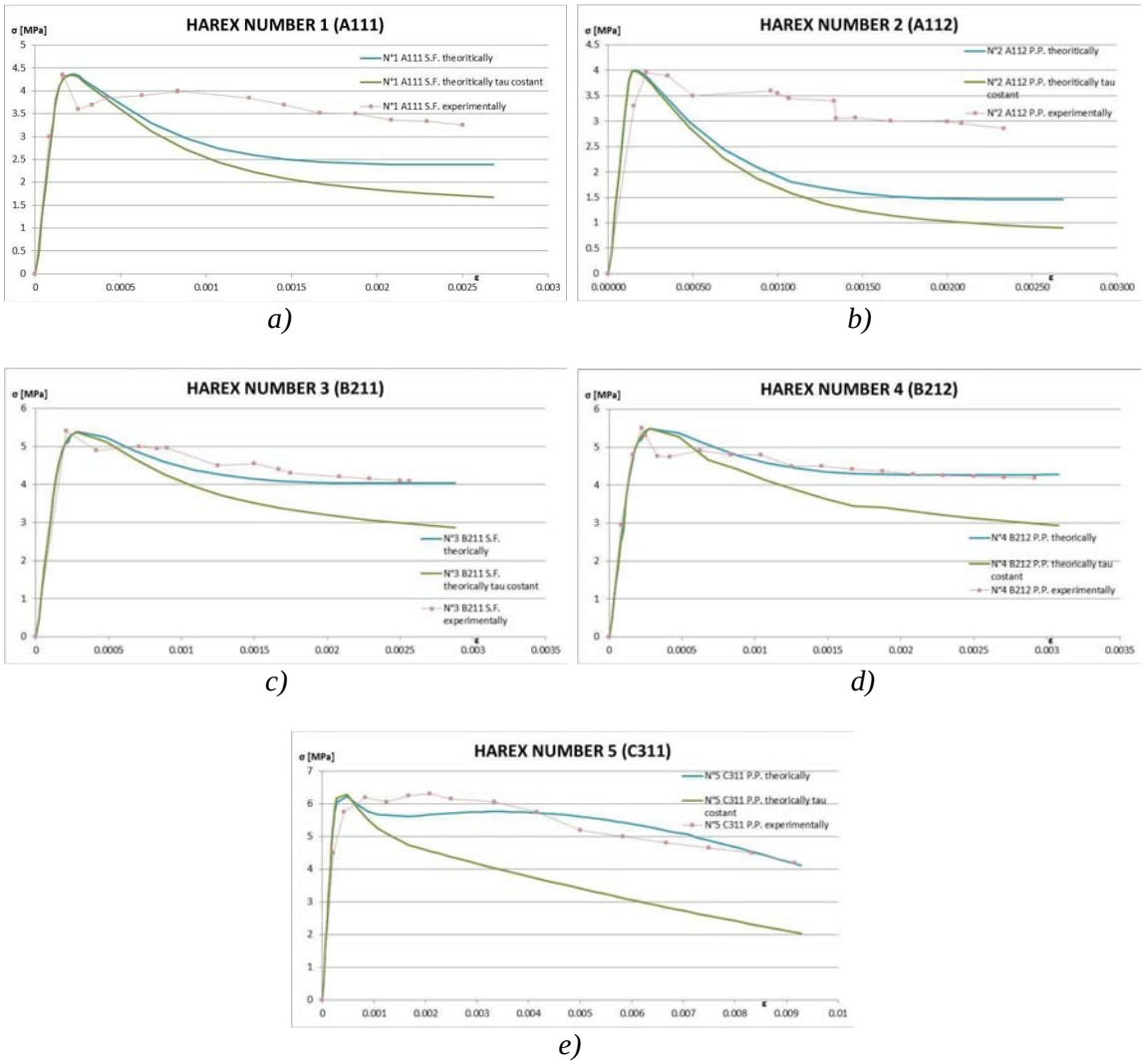

Fig. 3.11 *Confrontation of the models*

In the overall tests, the rising slope of the pull-out branch obtained when using the hardening parameter β is important in describing the characteristic pull-out behaviour, whereas it is mostly negligible in the debonding stage and in the maximum stress value.

3.3 Probability distribution

Up to this point the same type of probability density function for the orientation angles of the fibres, as the one suggested by Li [6], was considered. A research about different type of distribution used by others authors led to probability density functions that needed a calibration of the parameters through tests on specimens or analysis of experimentally data. Sometimes, the complexity of these equations require numerical integration in obtaining the solution. This subsequently leads to increase of the computational cost and a decrease of the model control. For these reasons some simple probability density functions were tested in order to improve the understanding of the influence of fibre orientation on the crack-bridging response. Modifying the probability density function that describes the distribution of fibre orientation leads to a different analytical solution of the crack-bridging stress than that obtained by Lin and Li [1]. In the derivation of the new solution, most of the assumptions and simplifications employed by Lin and Li [1] were maintained.

3.3.1 Analytical derivation

In order to insert a different probability density function in the model equations (2.12/14), it is first necessary separate the integrals and isolate the part relating to the probability distribution (appendix I). In the original model of Lin and Li [1], a uniform probability density function of the fibre orientation, $p(\varphi) = \sin(\varphi)$, was considered. It can be observed that this distribution function is independent of the pull-out force and it is described by the coefficient g/2 (appendix II), where g has the meaning already seen in the previous chapters (2.20). Two additional types of probability density functions were tested in this work; a constant distribution and a bi-linear distribution.

3.3.1.1 Constant distribution

For expediency a constant distribution was first chosen, which considers an equal probability for any fibre orientation to occur.

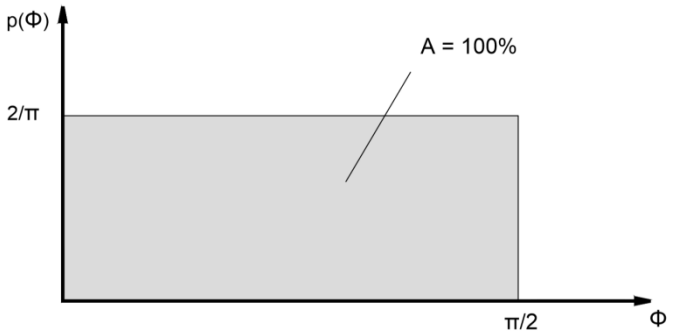

Fig. 3.12 *Constant probability density distribution function*

$$p|_{constant} = \int_0^{\frac{\pi}{2}} \int_0^{z_0 cos\emptyset} \frac{2}{\pi} e^{f\emptyset}\, dz' d\emptyset \tag{3.1}$$

$$p|_{constant} = \frac{2}{\pi}\left[\frac{e^{f\emptyset}}{(1+f^2)} \cdot (sin\emptyset + f cos\emptyset)\right] \tag{3.2}$$

The function is completely independent by the orientation angle φ, as is expected from a constant distribution. In the derivation of the function the z_0 element (I.4) was neglected because it is independent of the probability density distribution (as demonstrate in appendix I). The analytical solution given in (3.2) was verified by comparing the results obtained analytically with results obtained employing a numerical integration Mathcad built-in function (Fig.13):

variables

$f := 0.6 \qquad \phi_1 := 0 \qquad \phi_2 := \frac{\pi}{2.1} \qquad \phi_3 := \frac{\pi}{2}$

costant distribution

$c := \frac{1}{\phi_3} = 0.637$

$Ci := c\left(\int_{\phi_1}^{\phi_3} \cos(\phi)\cdot e^{f\cdot\phi}\, d\phi\right) = 0.92$

$Ca := c\left[\frac{e^{f\cdot\phi_3}}{(1+f^2)}\cdot(\sin(\phi_3)+f\cdot\cos(\phi_3)) - \frac{e^{f\cdot\phi_1}}{(1+f^2)}\cdot(\sin(\phi_1)+f\cdot\cos(\phi_1))\right] = 0.92$

Fig. 3.13 *Mathcad integral solution for the constant probability density distribution function*

3.3.1.2 Linear distribution

This type of distribution is characterized by the presence of a dominant angle " Φ_2", which is the fibre orientation angle with the higher probability. In order to have the maximum control possible, the Mathcad algorithm was built with the possibility of choosing the dominant angle. The bi-linear equation that describe the probability distribution is:

$$f_1(\emptyset) = m_1 \cdot \emptyset \quad ; \quad f_2(\emptyset) = m_2 \cdot \emptyset + a_2 \tag{3.3}$$

$$m_1(\emptyset_2) = \frac{4}{\pi} \cdot \frac{1}{\emptyset_2} \quad ; \quad m_2(\emptyset_2, \emptyset_3) = \frac{4}{\pi} \cdot \frac{1}{(\emptyset_2 - \emptyset_3)} \quad ; \quad a_2(m_2, \emptyset_3) = -m_2 \cdot \emptyset_3 \tag{3.4}$$

where:

Φ_2 = dominant angle

$\Phi_3 = \pi/2$ (fibre parallel to the crack direction)

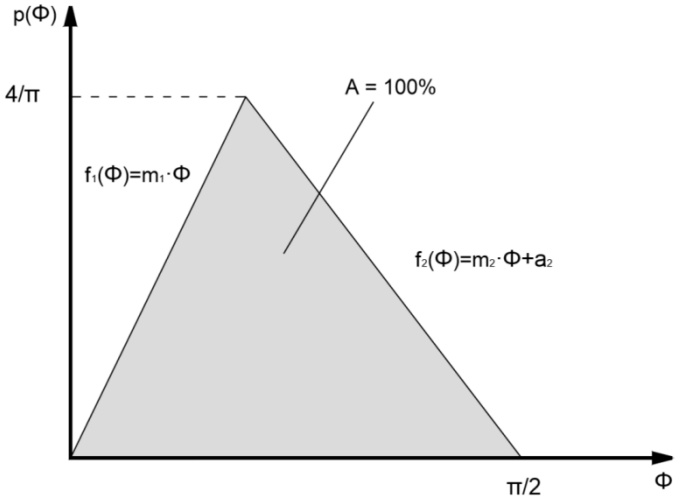

Fig. 3.14 *Constant probability density distribution function*

$$p|_{linear} = \int_0^{\frac{\pi}{2}} \int_0^{z_0 cos\emptyset} (f_1(\emptyset) + f_2(\emptyset)) e^{f\emptyset}\, dz' d\emptyset \tag{3.5}$$

$$\begin{aligned} p|_{linear} = {} & m_1 \left[\frac{e^{f\emptyset}}{(1+f^2)} \cdot \left(sin\emptyset \cdot \emptyset + cos\emptyset \cdot (1 + f\emptyset) \right) - \frac{2f e^{f\emptyset}}{(1+f^2)^2} \cdot (sin\emptyset + f cos\emptyset) \right] + \\ & m_2 \left[\frac{e^{f\emptyset}}{(1+f^2)} \cdot \left(sin\emptyset \cdot \emptyset + cos\emptyset \cdot (1 + f\emptyset) \right) - \frac{2f e^{f\emptyset}}{(1+f^2)^2} \cdot (sin\emptyset + f cos\emptyset) \right] + \\ & a_2 \left[\frac{e^{f\emptyset}}{(1+f^2)} \cdot (sin\emptyset + f cos\emptyset) \right] \end{aligned} \tag{3.6}$$

The linear distribution allow to control possible parameters that may influence the orientation angles because is possible to set the main angle; thus, once know how some parameters influence the fibres orientation, is possible set the main angle in order to consider boundary conditions. The analytical solution when employing a linear distribution was verified with the Mathcad built-in numerical integration solver (Fig. 3.15).

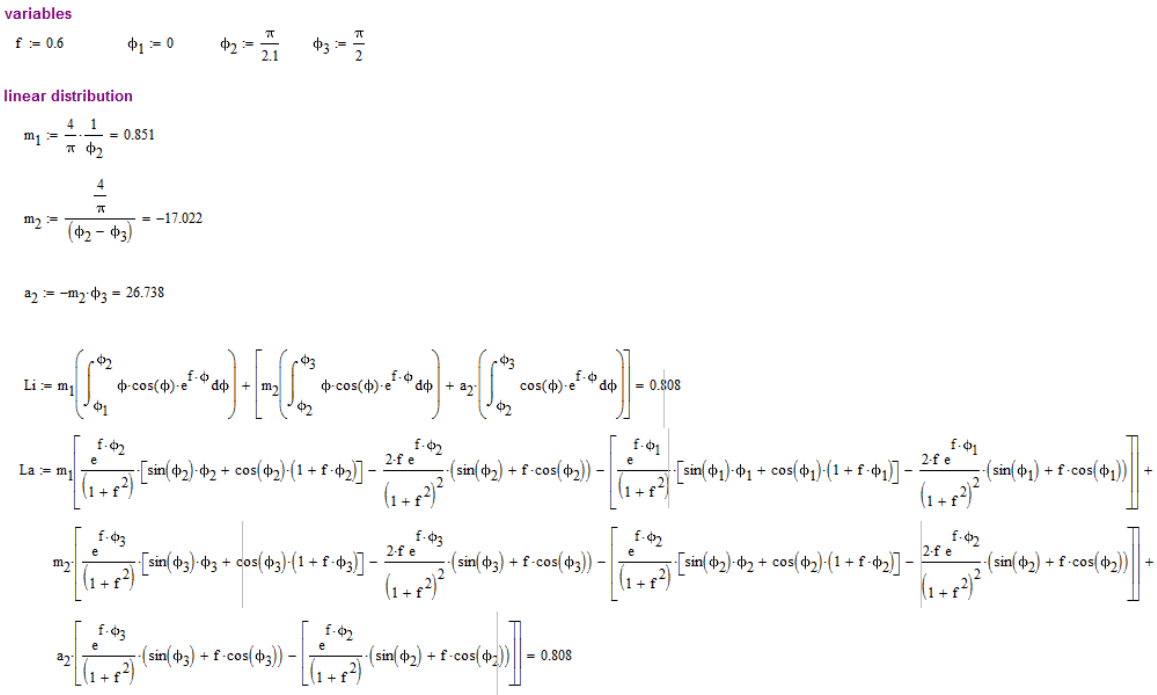

Fig. 3.15 *Mathcad integral solution for the linear probability density distribution function*

3.3.2 Results comparison

Numerical analyses were carried out with the model employing the two probability density functions described above and the results were compared against the same set of data from Lin and Li [8]. After the firsts results, additional analyses were performed with an aim to improve the understanding of the model response.

3.3.2.1 Constant parameters values

The influence of the different types of probability distributions on the predict crack-bridging response is next considered, in particular the predicted behaviour during the debonding stage, the predicted peak crack-bridging stress and the predicted pull-out

behaviour respectively. In this study the values of the fibre-matrix interface parameters (β, τ_0) were kept unchanged and only the probability density function was modified. For the linear distribution a dominant orientation angle of $\phi_2 = 45°$ was chosen.

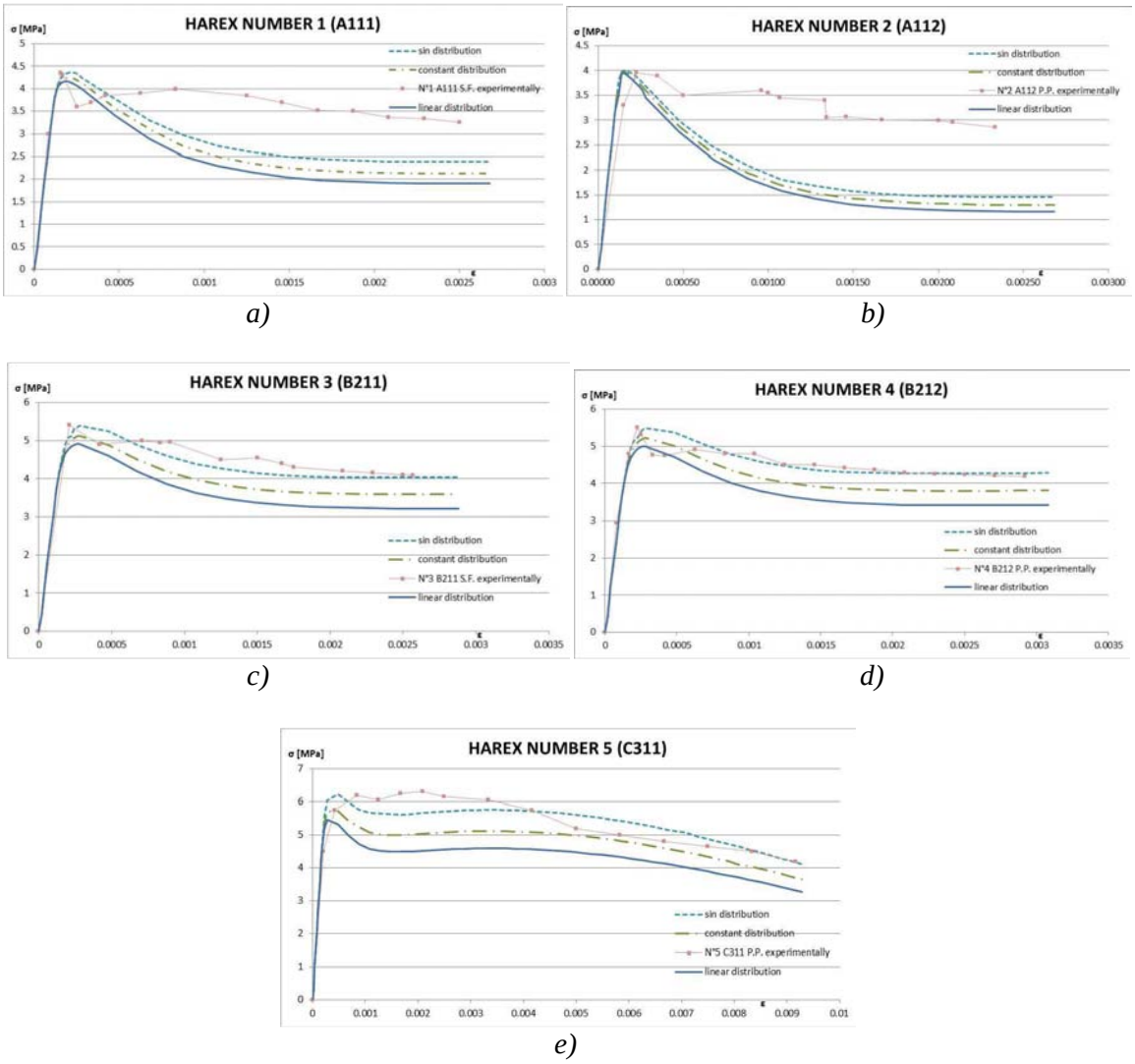

a) *b)* *c)* *d)* *e)*

Fig. 3.16 *Different probability distribution's functions*

In the debonding stage the predicted behaviour is practically the same for all the probability distribution considered. Indeed, before matrix cracking initiated, the contribution of the fibres to stiffness of the fibre reinforced composite is negligible and, thus, their angle orientation as well. A first important difference between the various probability density functions is in the maximum stress value at the end of the debonding stage. As the results in Fig. 3.16 show this is maximum for the sin(ϕ) distribution and minimum for the linear distribution. Furthermore this maximum stress increases with V_f (Fig. 3.16e). In the pull-out stage, the apparent parallelism of the branches suggests a

small influence of the angles orientation in the hardening behaviour. The dominant orientation angle chosen influences the numerical values but not the trend of the model. In reference to the graphs above, it is possible to conclude that the different probability density functions have a noticeable effect on the stress at the end of the debonding stage and only a marginal effect on the pull-out trend.

3.3.2.2 Different parameters values

Once the influence of the fibre orientation on the predicted behaviour was studied, it is required to understand if the crack bridging model, with different values of the fibres parameters, should employ a particular distribution of fibre orientation. To do that was found for each probability density function considered, the best fitting values for β, τ0 and aef were obtained and compared. For the linear distribution, a domination angle φ2 = 18° was chosen in order to have a small influence of the snubbing effect that can misunderstanding the study.

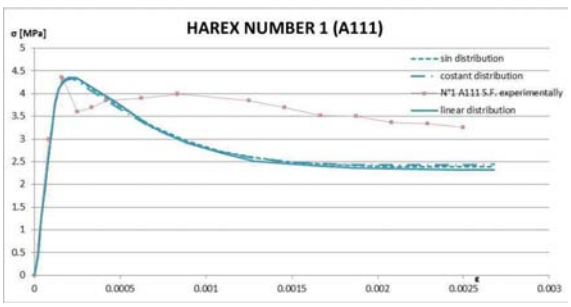

a)

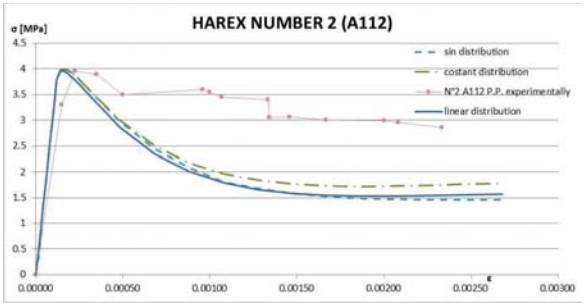

b)

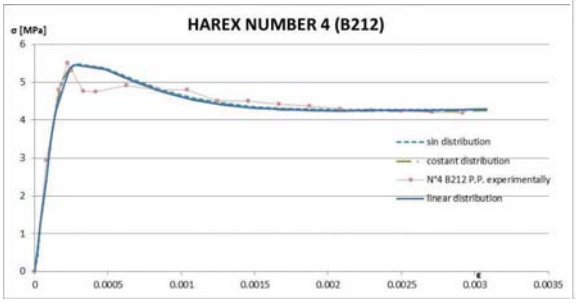

c)

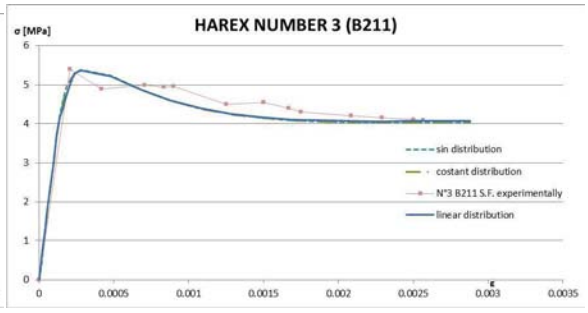

d)

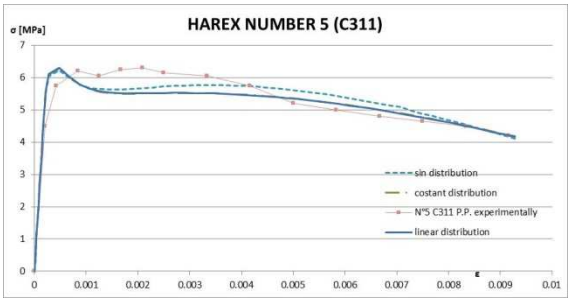

e)

Fig. 3.17 *Best fitting with different probability density distribution functions*

It can be observed that there are only minor differences between the prediction of the model employing different probability density functions, in particular in the debonding stage and for the maximum stress value. More significant but still marginal differences are present in the pull-out branch where the influence of the fibre is more important. The slope of the branch varies for the different probability density distribution functions (Fig. 3.17b,e). A more extensive study, including experimental observation regarding real distributions of fibres, is required in order to choose a probability function suitable for simulating specific experimental tests. Nevertheless, a set of suitable model parameters has been identified following the proposed study (table 3.4).

Table 3.4 *Model setting parameters*

Volume fraction	**Specimen**	**Probability density distribution's function**	**β**	**τ_0 [MPa]**	**a_{ef}**
2 %	A111	Sin(ϕ)	0.23	3.3	0.85
		Constant	0.28	3.57	0.85
		Linear	0.22	4.22	0.85
2 %	A112	Sin(ϕ)	0.26	1.8	0.895
		Constant	0.49	2.05	0.85
		Linear	0.49	2.1	0.85
3 %	B211	Sin(ϕ)	0.22	3.51	0.85
		Constant	0.22	3.95	0.85
		Linear	0.22	4.45	0.88
3 %	B212	Sin(ϕ)	0.23	3.67	0.85
		Constant	0.23	3.3	0.85
		Linear	0.23	4.6	0.88
6 %	C311	Sin(ϕ)	0.265	2.07	0.75
		Constant	0.188	2.12	0.85
		Linear	0.185	2.5	0.85

The different probability distributions considered haven't a limited influence on the range of the parameters values for the case of steel fibres. A proportional relationship, between

the different functions is evident in the τ_0 factor whereas for the β parameter a constant-linear common match is apparent.

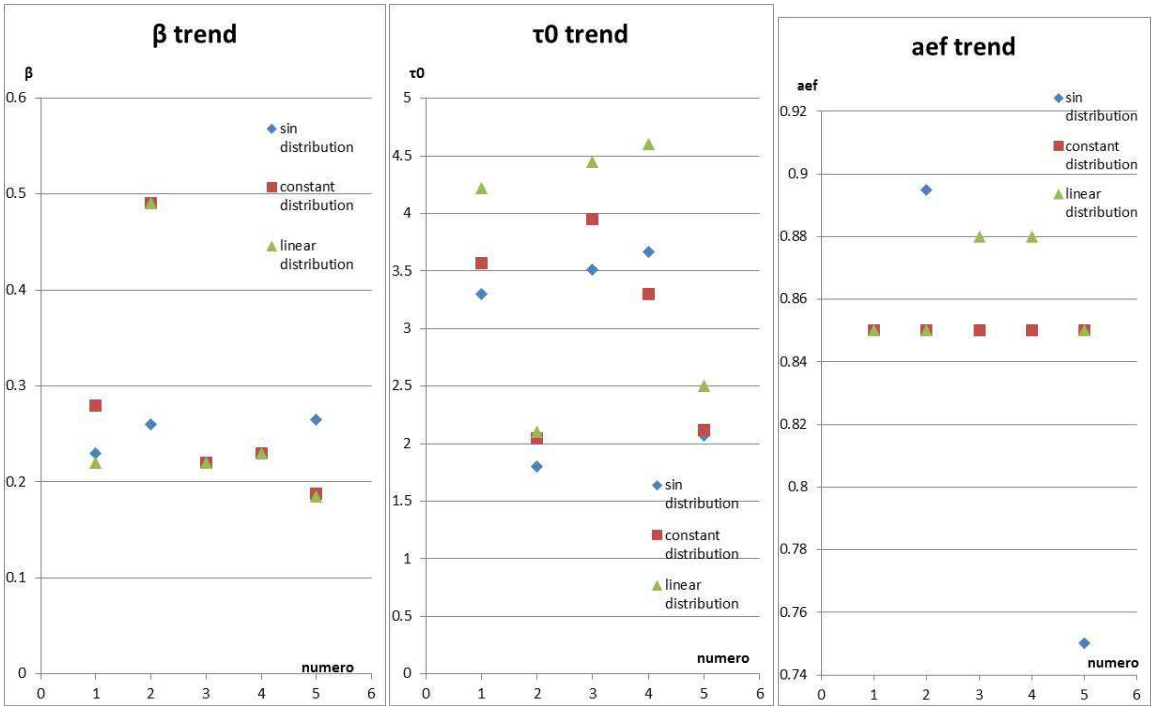

a) *b)* *c)*

Fig. 3.18 *Main parameters confrontation respect the different probability density functions and respect volume fractions*

The charts above confirm a good match of the constant and linear probability functions in the case of the hardening parameter β (Fig. 3.18a). Apart for the A111 specimen, the results are in agreement. An interesting relationship is shown in the τ_0 trend (Fig. 3.18b) where a proportional increment link the different probability functions, in fact the lower value for the same specimen is, practically always, the sin distribution, the middle ones is the constant distribution and the higher is the linear distribution. This behaviour may be attributed to the greater influence of the probabilistic distribution in the top stress value than in the pull-out behaviour. Finally the a_{ef} parameter is stable around the 0.85 value for both the new probability density functions.

3.3.2.3 Linear distribution

Up to this point a linear probability distribution with a particular dominant orientation was considered. The aim in this section is to understand how the behaviour and the

response of the model vary if the dominant angle of the linear probability density function changes. For this, three different dominant angles were considered whereas the values of the remaining model parameters from the case $\phi_2 = 18°$ were employed.

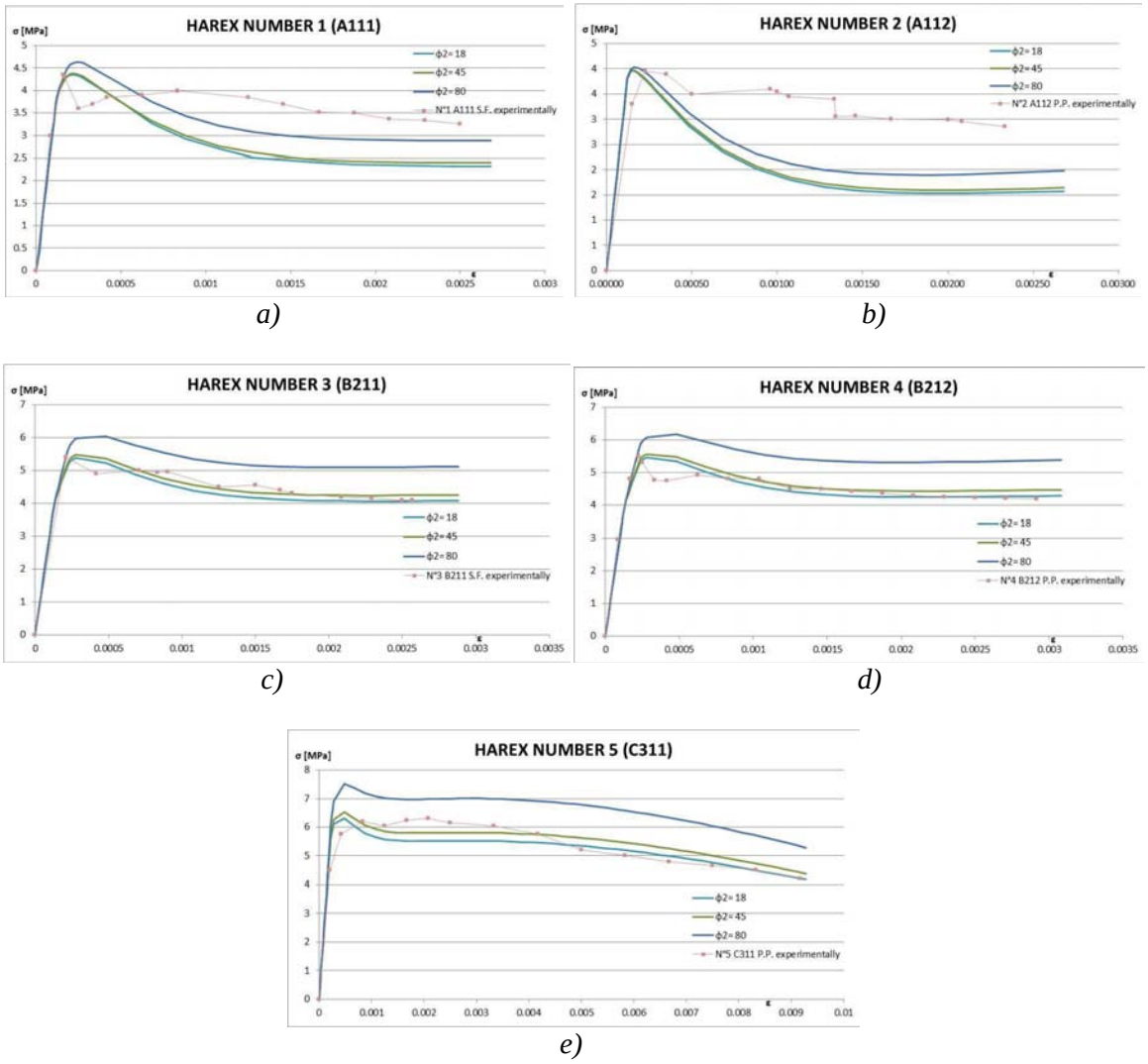

Fig. 3.19 *Linear distribution with different main angle*

The charts above are quite exhaustive about the different behaviour at the varying of the dominant angle, because with every volume fraction the dominant angle to obtain the higher response is the $\phi_2 = 80°$, thus with the fibres mostly orthogonal at the force direction. Indeed, the higher force needed for the pull-out is due to the snubbing effect [6]. It should be mentioned that the model does not consider the spalling of the concrete if the angle is wide so the snubbing coefficient should be calibrated in consideration of that. The effect of the different angle consists in a shift of the pull-out branch and is this shift highest for the $V_f = 6\%$ (Fig. 3.19e). The advantage of this probability density distribution

function is that it is easy to calibrate, through the dominant angle, if a relation with the others boundary conditions will be found.

3.3.3 Volume fraction influence

The distribution of the angles orientation and location is influenced by some boundary condition like contact between the fibres, binder boundary influence, casting flow direction [15][9]. The influence of boundary conditions can be significant and therefore a better understanding of it is beneficial. A first step involved a literature survey of experimental and numerical studies [9] investigating this problem. This research leaded to some consideration about parameters like aggregate dimension, concrete flow shape [15] or specimen dimension but not about parameters controllable in the numerical model at issue. Liu, Li, Du and Cui [9] investigated a possible relation between the fibre volume fraction and the fibre orientation (Fig. 3.20).

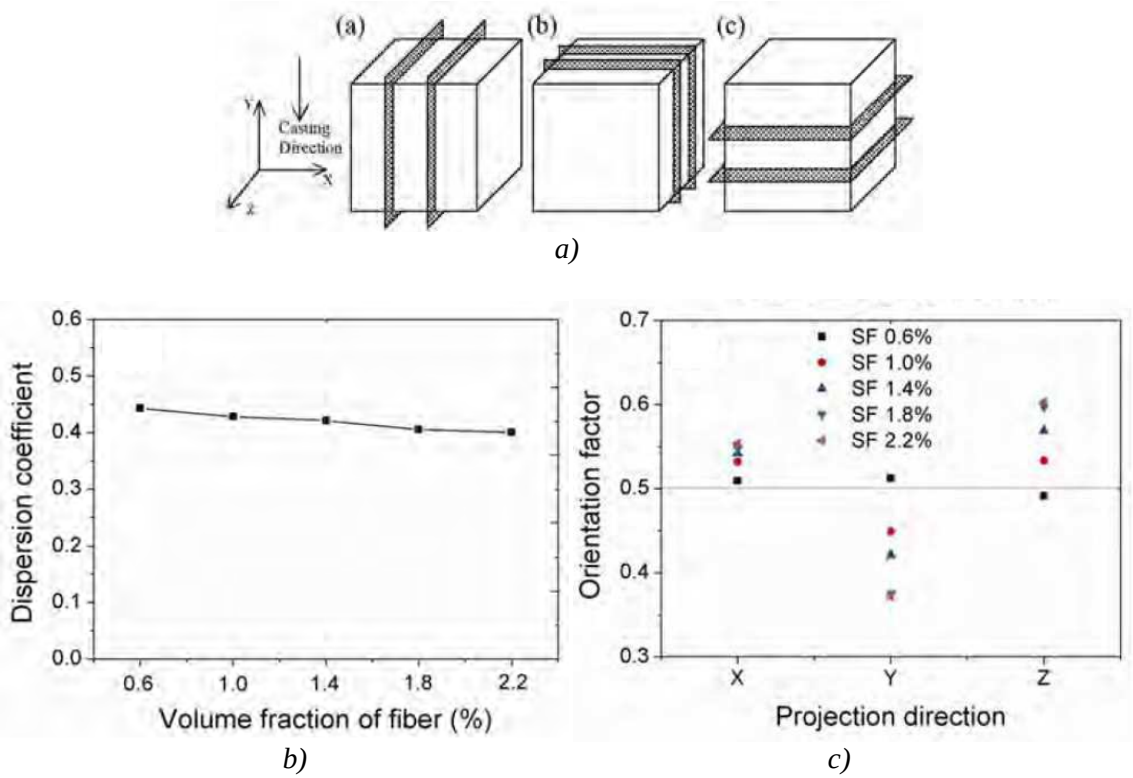

Fig. 3.20 *Volume fraction influence. The dispersion coefficient and the orientation factor are 2 values to describe the respective parameters variation, a 0.5 value means equal distribution in all the directions*

A small variation of the dispersion coefficient with volume fraction observed in Fig. 3.20b. This variation could be attributed to factors like binder boundary condition or casting flow direction. In order to get a better understanding regarding the relationship between the volume fraction and the fibre distribution function and understand the influence of the boundary condition (i.e. casting flow direction) a numerical parametric study was carried out in which the predicted responses obtained using the three different probability density functions considered in this chapter were compared for various fibre volume fractions. The values of the parameters used for the sin and constant distribution were the average values obtain from all the specimens, whereas, in the case of the linear probability density function the mean of the two average values of the sin and constant distribution were employed. These are given in table 3.5.

Table 3.5 *Volume fraction study mains parameters*

Probability density function	β	τ_0 [MPa]	a_{ef}
Sin(ϕ)	0.235	3.07	0.8613
Constant	0.305	3.2175	0.85
Linear	0.27	3.14	0.8556

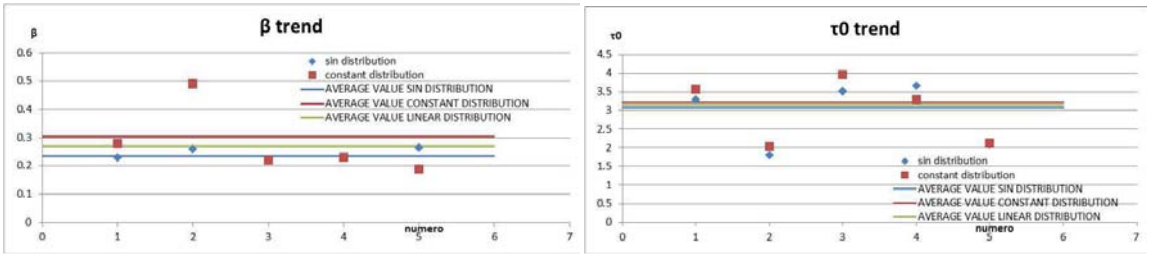

a) b)

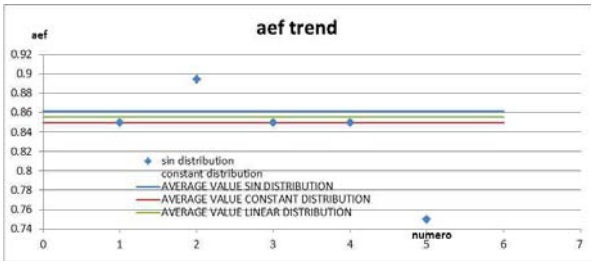

c)

Fig. 3.21 *Average values*

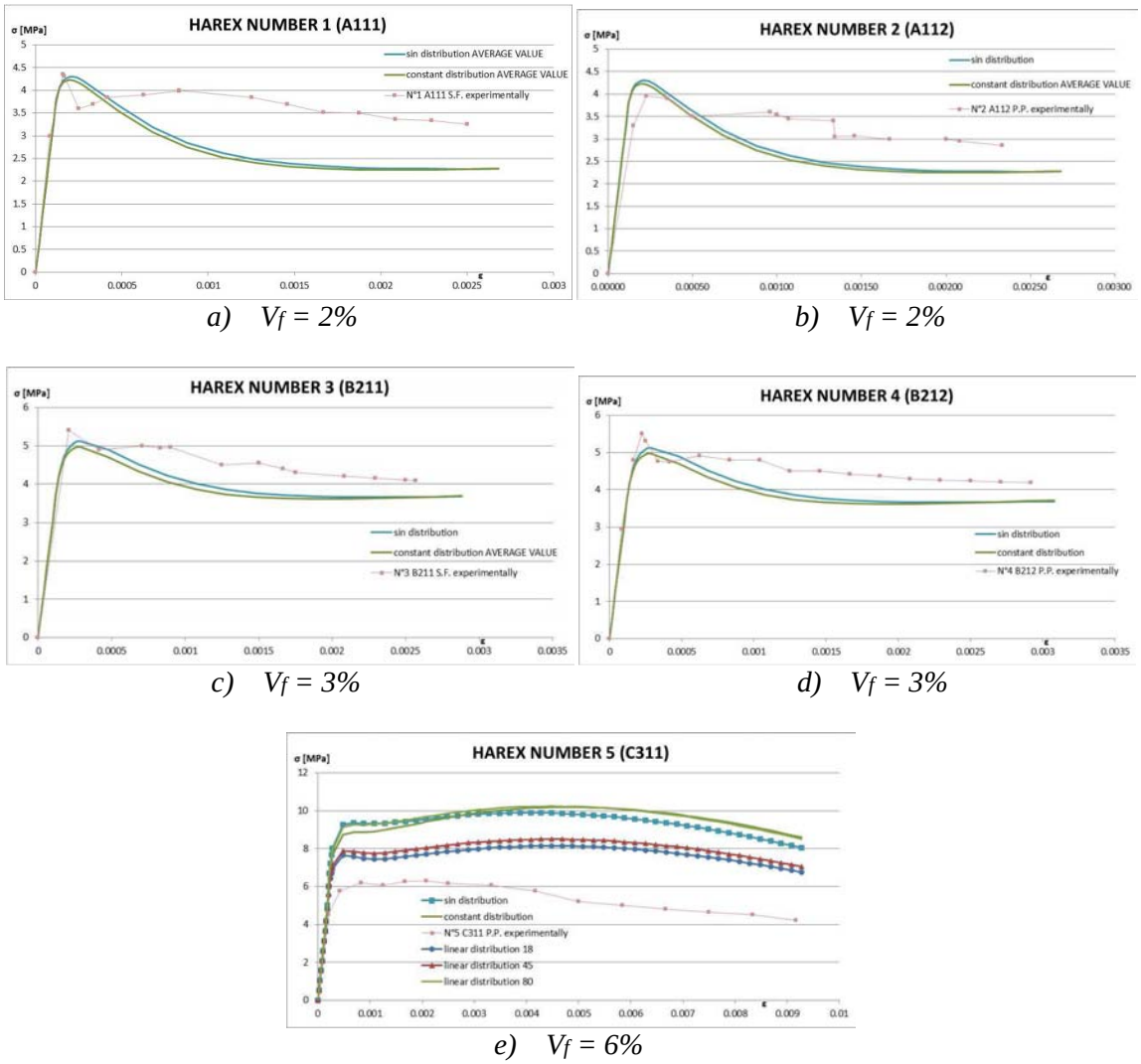

a) V_f *= 2%* *b)* V_f *= 2%*

c) V_f *= 3%* *d)* V_f *= 3%*

e) V_f *= 6%*

Fig. 3.22 *Volume fraction influence in the probability distribution's function*

The results of the study, presented in Fig. 3.22 show a good match between the predicted and experimental responses in the case of sin and constant function for low level of volume fraction (Fig. 3.22a,b,c,d) and a bad fit with the higher volume fraction specimen. Even if the previous considerations suggest a change of probability distribution's function the linear distribution used to fit the V_f = 6% don't lead to a satisfying fit as well. Thus is not possible say that there is a relation between volume fraction and the type of probability density distribution functions, and, the bad fit observed in Fig. 3.22e, could be due to other factors that have not been included in the analytical model employed in this study.

Chapter 4

Pull-out of hooked end fibres

In this chapter an analytical model is proposed that describes the pull-out of steel fibres with hooked ends. An energy approach and small-displacement mechanics theory was employed in deriving an analytical expression of the force required to pull-out a single steel fibre with a hooked end. The formulation was implemented in a Mathcad program to describe, together with Lin and Li model for straight fibre, the force-displacement relationship of single fibre pull-out test.

4.1 mechanical model

The main purpose of this analytical model is use simple equations to describe the straightening of fibres' hooks. For this, equations from basic solid mechanics theory are employed. Even if the dimension and type of problem do not allow a solution using relationship based on simple mechanics, studying the phenomena related to the problem and the application of few but important assumptions can lead to a good solution.

4.1.1 problem setting and assumptions

Like in every model, the first step is understanding the physical problem. Once the main mechanisms and phenomena are understood, it is possible focus the attention and the assumptions on it. Indeed, to keep the model simple, few but important assumptions are needed. A set of simplifying assumptions were employed in the formulation of the model. This assumption keep in account the semicircular geometry of the hook as shown in Fig. 4.1. The first assumption was consider the influence of the hook, in the pull-out force, happening on its onset (Fig. 4.1). In this region occurs the deformation that lead to the straightening of the fibre, in fact it is called “deformable region of the hook”. Furthermore this part of the fibre moves along the hook as the fibre is pulled out. It is further assumed that it is only this region of the hook that undergoes plastic deformations, whereas the rest of the fibre is subjected to the fibre-matrix frictional contact (with slip-hardening behaviour). This essentially means that the part of hook behind the contact point simply slides in the channel created in the matrix.

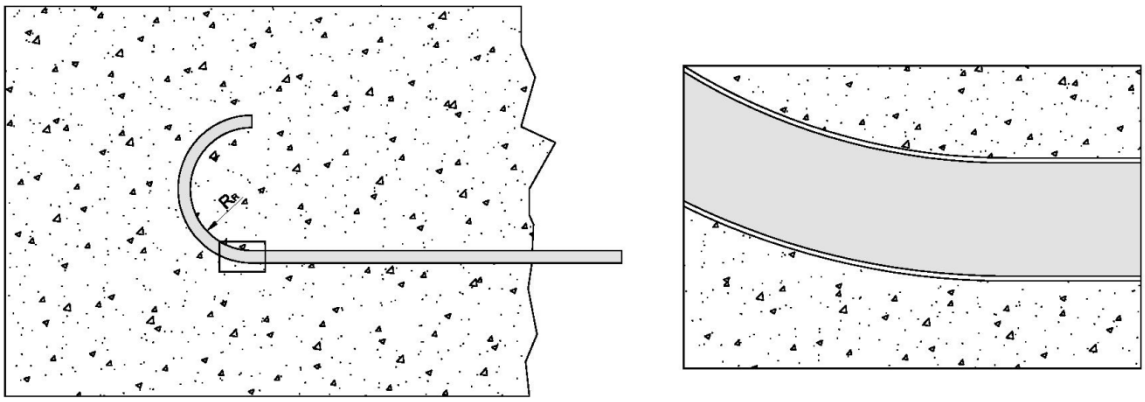

Fig. 4.1 *Embedded fibre schematization, with draw attention to the deformation region of the hook*

Another assumption is to consider the cementitious matrix initially non deformable. This assumption, in agreement with the work of Lin and Li [1] for straight fibre, could be quite strong if we consider generic geometries of the fibre. This assumption means that the contact point is at the beginning of the hook. Thus, in the rest of the hook, there is just matrix-fibre contact friction. During the fibre displacement increasing, as the tension as the deformation in the deformable region of the fibre increase. The stress profile in this section is assumed to follow a linear distribution, as the one given by the De Saint Venant theory (Fig. 4.2). For simplicity, the principles of small displacement mechanics theory are assumed to apply. The stress variation is linear until the maximum value reaches the yield stress.

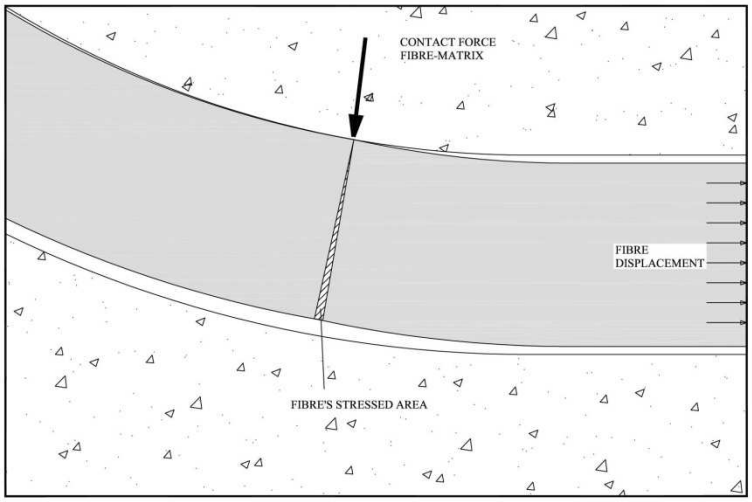

Fig. 4.2 *Linear stress distribution at the beginning of the pull-out stage*

The fact that after a small slip the plasticized section is developed at the beginning of the fibre is a non deformable matrix assumption's effect (Fig. 4.3).

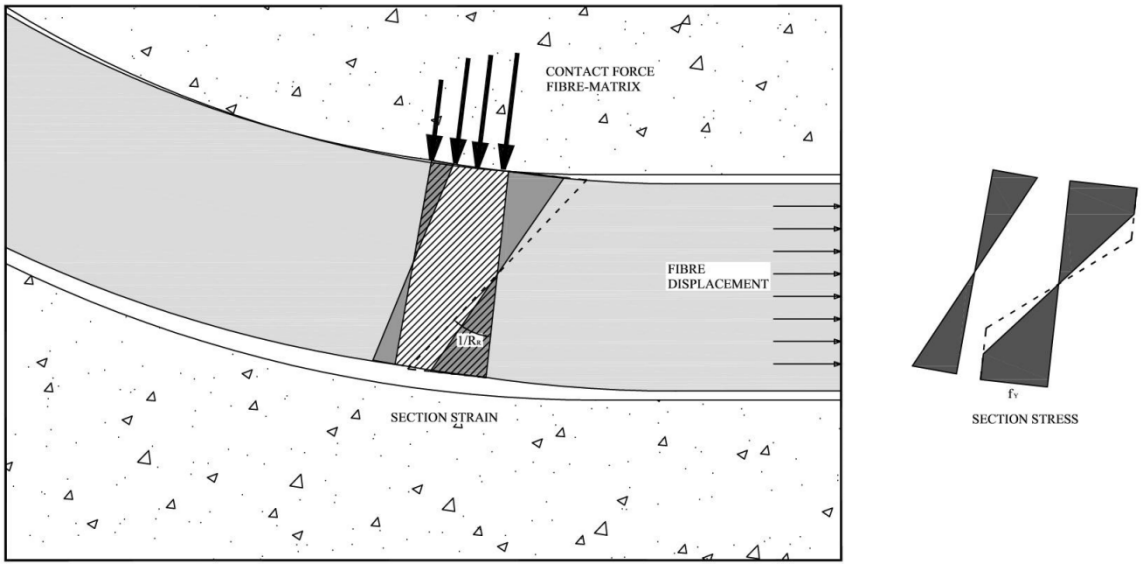

Fig. 4.3 *Stress arise in the fibre section*

Since all plastic deformations occur at the beginning of the hook, the small deformation theory can be applied. If the matrix was completely non deformable the deformable region of the fibre is very small, theoretically infinitesimal. However for the implementation in a Mathcad calculation sheet, a finite length is required. These assumptions imply that any time there is a curvature change, a plastic hinge is developed. The pull-out force needed to straighten the hook, was calculated by employing energetic considerations:

$$\int \sigma\varepsilon \, dx \, dy \, ds \tag{4.1}$$

$$\frac{1}{2}\int \sigma\varepsilon \, dx \, dy \, ds \tag{4.2}$$

$$L_i = L_e \tag{4.3}$$

Where:

"dx" and "dy" are the cross section dimensions

"ds" is the longitudinal direction

Whereas (4.1) represents the plastic internal energy and (4.2) represents the elastic internal energy, (4.3) represents the theorem of the virtual works. With small

deformations assumption (4.4), the hook deforms until the curvature reaches the value $1/R_R$ to became straight.

$$\frac{1}{R_R} = \frac{\frac{d^2v}{dx^2}}{\left[1+\left(\frac{dv}{dx}\right)^2\right]^{2/3}} \cong \frac{d^2v}{dx^2} \tag{4.4}$$

Where:
"R_R" is the radius of the hook.

When the curvature reaches the value for straightening, only part of the cross section has undergone plastic deformation. Thus the total energy is given by the sum of the elastic energy (till x) and the plastic energy (from x till $R=d_f/2$) as shown in Fig. 4.4. "x" represents the distance of the elastic area from the neutral axis of the section. A circular section was chosen here because most of the commercially available steel fibres has this type of cross-section. However, this assumption leads to rather complex mathematical expressions that subsequently need to be integrated.

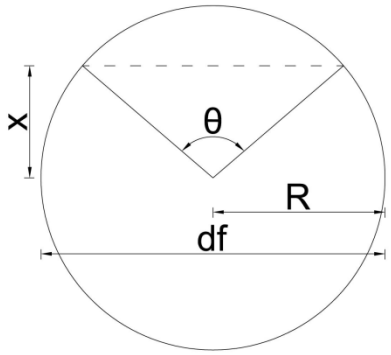

Fig. 4.4 *Circular section geometry*

The non linearity of the material adds further complexity to the integration of the internal energy. Indeed the integral was split in two parts as explain subsequently.

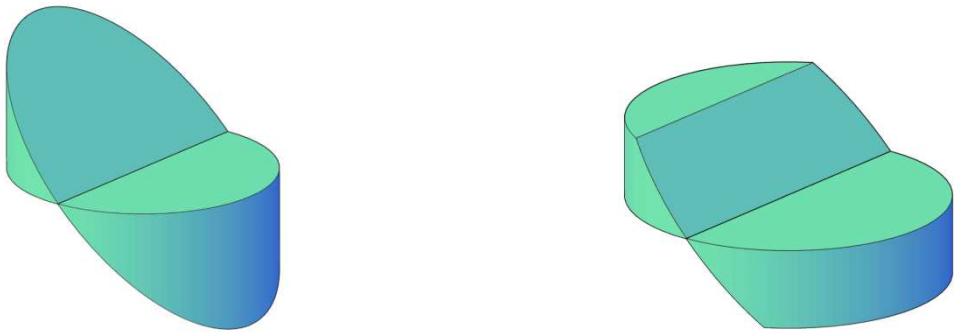

a) *b)*

Fig. 4.5 *Cross circle section strain distribution (a), cross circle section stress distributions (b)*

The steel is next assumed to have a perfectly plastic behaviour as illustrated in Fig. 4.6. This type of behaviour is quite common for steel. Nevertheless the steels used for fibres are usually more strength than the structural steel.

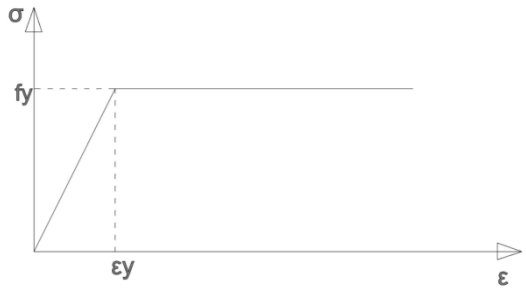

Fig. 4.6 *Material's perfect plasticity relationship used for the internal energy*

4.1.2 Internal energy

The conservation of energy (4.3) allows to find the relationship between pullout force and bending plasticization's moment. The first step is to calculate the maximum plastic deformation needed to bend the fibre until the curvature $1/R_R$ is reached. This is obtain from the strain distribution in the deformation region of the hook.

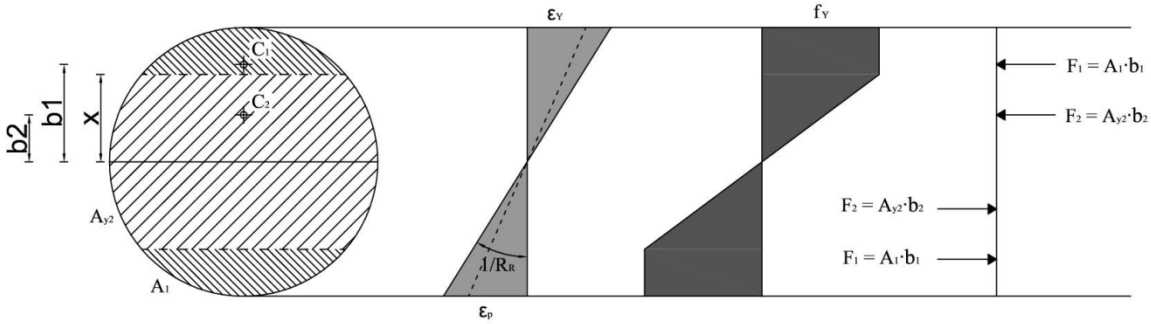

Fig. 4.7 *Geometrical and mechanical relationship to derive the plastic bending moment of the fibre*

$$\varepsilon_p = \frac{R}{R_R} \quad , \quad R_R = \frac{x}{\varepsilon_y} \tag{4.5}$$

thus

$$x = \frac{\varepsilon_y}{\varepsilon_p} R \tag{4.6}$$

Once the plastic area in the circular cross-section is determined it is possible to calculate the bending moment that would cause the fibres up to "x" to undergo plastic deformation (Fig 4.7). This relationship is split in the elastic part (4.8) and in the plastic part (4.9).

$$Li = \left[2 f_y \frac{Ay1}{R}\left(\varepsilon_p - \frac{\varepsilon_y}{2}\right) + \frac{Mp^2}{2\,E\,(2I)^2}(2\,I2)\right] ds \tag{4.7}$$

$$Li_e = \frac{Mp^2}{2\,E\,(2I)^2}(2\,I2) \tag{4.8}$$

$$Li_p = 2 f_y \frac{Ay1}{R}\left(\varepsilon_p - \frac{\varepsilon_y}{2}\right) \tag{4.9}$$

Where:
"f_y" is the yield stress
"Ay1" is the volume of the strain as calculate in appendix III
"ε_P" is the maximum strain
"ε_y" is the yield strain
"M_P" is the plastic moment
"I" is the inertia moment of half section as calculate in appendix III
"I2" is the inertia moment of partial half section as calculate in appendix III

All the geometrical relations used to evaluate the integral over the circular section, given in (4.7) are explained in appendix III. Several observation regarding the plastic energy in equation (4.9) are given below:
- it is multiplied by 2 since both the top and the bottom half of the circular cross section are considered
- 1/R is to no-dimensional the integral
- $\varepsilon_p - \varepsilon_y$ is the plastic strain, it means that only the strain after the plastic deformation value is considered

- $+\frac{\varepsilon_y}{2}$ considers the elastic strain in the circle segment and it is halved because the elastic energy definition is $\frac{1}{2}\int \sigma\varepsilon\, dx\, dy\, ds$

The equation (4.8) gives the bending moment's energy just until x. The relation derives from bending moment deformation energy with linear material's behaviour. It is multiplied 2 with the purpose of consider both the section's half part. In the equation (4.8) the moment distribution is considered constant because the error is negligible.
In the equations above the axial stress and strain given by the pull-out test are neglected. Indeed the neutral axis is in the middle of the section. This assumption was made because the magnitude of the axial stress is lower than the magnitude of the stress from the plastic bending moment.

4.1.3 External energy

The main external force is given by the pull-out force. Assuming an orthogonal orientation of the fibres with respect to the cross crack section the work is given by:

$$Le = P\, ds \tag{4.10}$$

A secondary, but not negligible, energy component is given by the friction caused by the contact point at the beginning of the fibre hooks. The bending moment required to straighten the fibre is quite high but the contact length is small (Fig. 4.2) thus even the arm of the moment. If the arm is small it means that the force has to be big. To evaluate the value of this force equilibrium and geometrical relationship is used (appendix III):

$$P_{\perp} = \sqrt{\frac{P}{R}M} \tag{4.11}$$

The orthogonal force equation (4.11) considers all the main parameters that influence the contact force. In fact it considers the hook geometry with the curvature "R", but even material and fibre features through the plastic moment "M". For the friction force a Coulomb coefficient was used:

$$P_{//} = P_{\perp}\mu \tag{4.12}$$

where:

"μ" is the friction coefficient

"$P_{//}$" is the friction force

The friction force's work is negative because the direction of the force and the displacement "ds" are opposite. However the displacement "ds" can be used because its length is short. Hence the curve length, due to the hook, in the friction force direction is confuse with its projection "ds". The external energy final relationship is:

$$Le = P\ ds - \sqrt{\frac{P}{R} M\ \mu\ ds} \tag{4.13}$$

4.2 FEM analysis

The energetic and mechanical model derived to describe the straightening of a hook is unique. The majorities of models used to describe the hooked end fibre pull-out behaviour are FEM models or empirical models. A similar approach to the one employed in this work was found in [10]. To gain a better understanding of the behaviour predicted by the proposal analytical model and to validate it, simple FEM models were created that simulate the pull-out of a hooked end steel fibre. These models reproduce the energy of deformation due to the plastic moment of a fibre that is simulate by a beam element, and the fibre and matrix stresses and strains during the fibre pull-out trough plate elements. The software used was Straus even if it does not have all the finite elements desiderable to obtain a fully comprehensive model, i.e. interface elements. This choice was made because the purpose of the FEM analysis in this thesis is to understand and validate the assumptions of the analytical model rather than to create a complete pull-out FEM model.

4.2.1 Internal energy FEM model

As mentioned before, the purpose of the FEM model is to validate the analytical relation for the plastic energy using the small deformation theory. The FEM model employs 1000mm long embedded beam element to characterize the fibre. It was loaded with a concentrate moment in the free end (Fig. 4.6a). For the symmetry of the problem the solution was found in the <x,y> plane. The geometrical characteristics of the cross section are described in Fig 4.6b.

a)

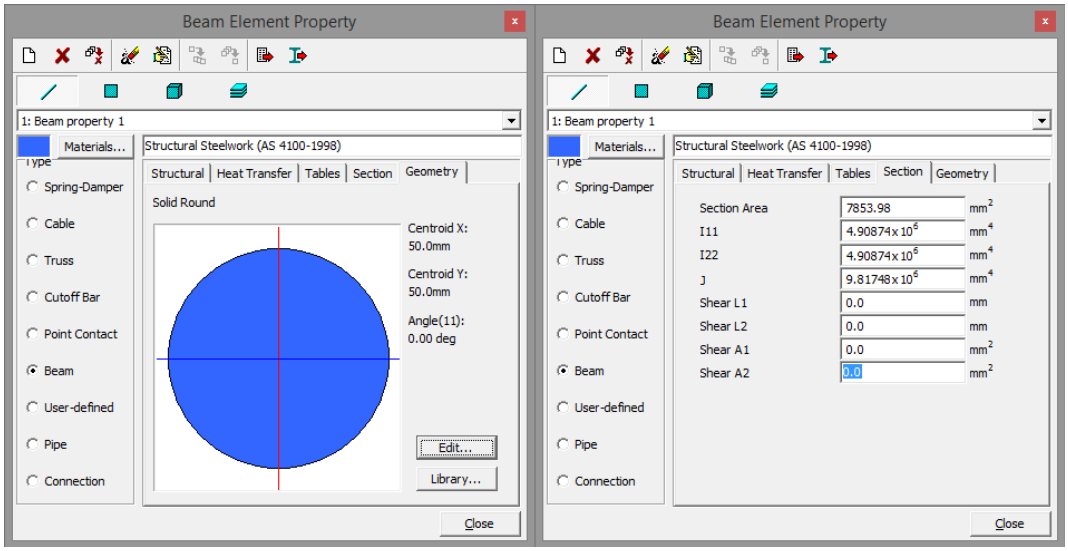

b)

Fig. 4.6 *Static scheme (a) and section geometry (b) used for the internal energy validation*

In order to consider the perfect plasticity behaviour of the material, a moment vs curvature table was made. Its function is to consider the plasticity of the material/cross-section. The moment-curvature relationship depends upon the geometry of the section. The relation illustrated in Fig. 4.7 representative for a circular cross-section.

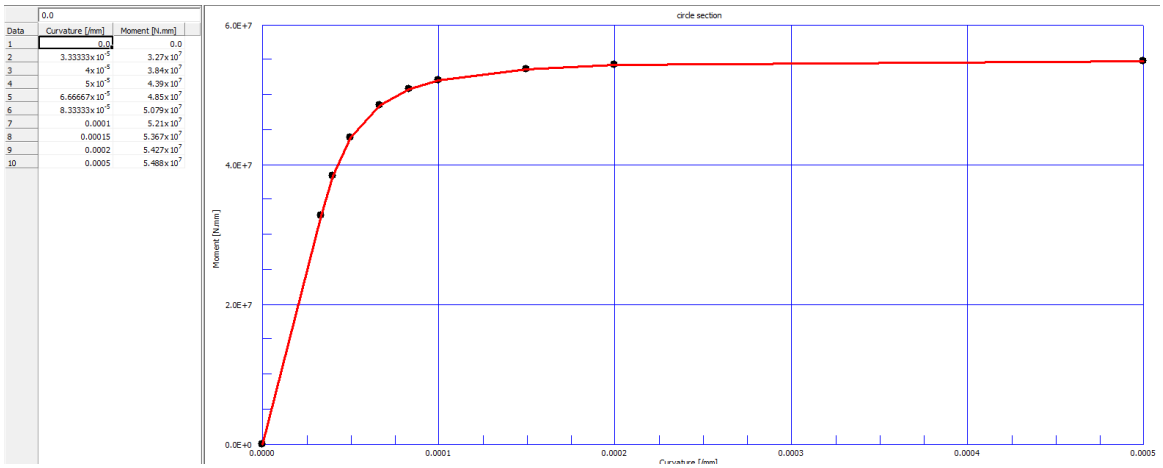

Fig. 4.7 *Moment vs curvature table*

For the solution, a non linear geometry solver with 10 steps was used. The plastic energy obtained with the FEM analysis is shown and compared with the analytical energy relationship (4.7) in table 4.1.

Table 4.1 *Models comparison respect different values of bending moment*

Moment [Nmm]	**Analytical Model energy [N]**	**FEM model energy [N]**	**Models rapport [Analytical/FEM]**
3,272e7	545	540	1.01
5.205e7	3945	3589	1.1
5.425e7	9695	8859	1.09
5.488e7	26419	25234	1.05

A reasonable match between the analytical and FEM results is observed. The values are not exactly the same but the difference is always less than 10%. Both methods used in obtaining the results in Table 4.1 have limitations however, the favourable comparison between the results suggests that the assumptions employed in the analytical model were reasonable.

4.2.2 Pull-out FEM model

The analytical model developed in this thesis takes into account the fact that the fibres undergo plastic deformations during the hook straightening and also the friction between the fibre and the matrix. These phenomena were considered of primary importance in reproducing the pull-out behaviour, as suggested by Zile [10]. In particular, a more comprehensive FEM model that simulates the pull-out of hooked-end fibres and described in [11] was used to understand all the different mechanisms during the pull-out phenomenon. As only limited data/results were available, the model [11] was rebuilt in Straus in order to gain a better understanding of the matrix effect and the fibre behaviour. A simple 2D finite element model was built for this purpose. Furthermore the problem symmetry was used to simplify the model.

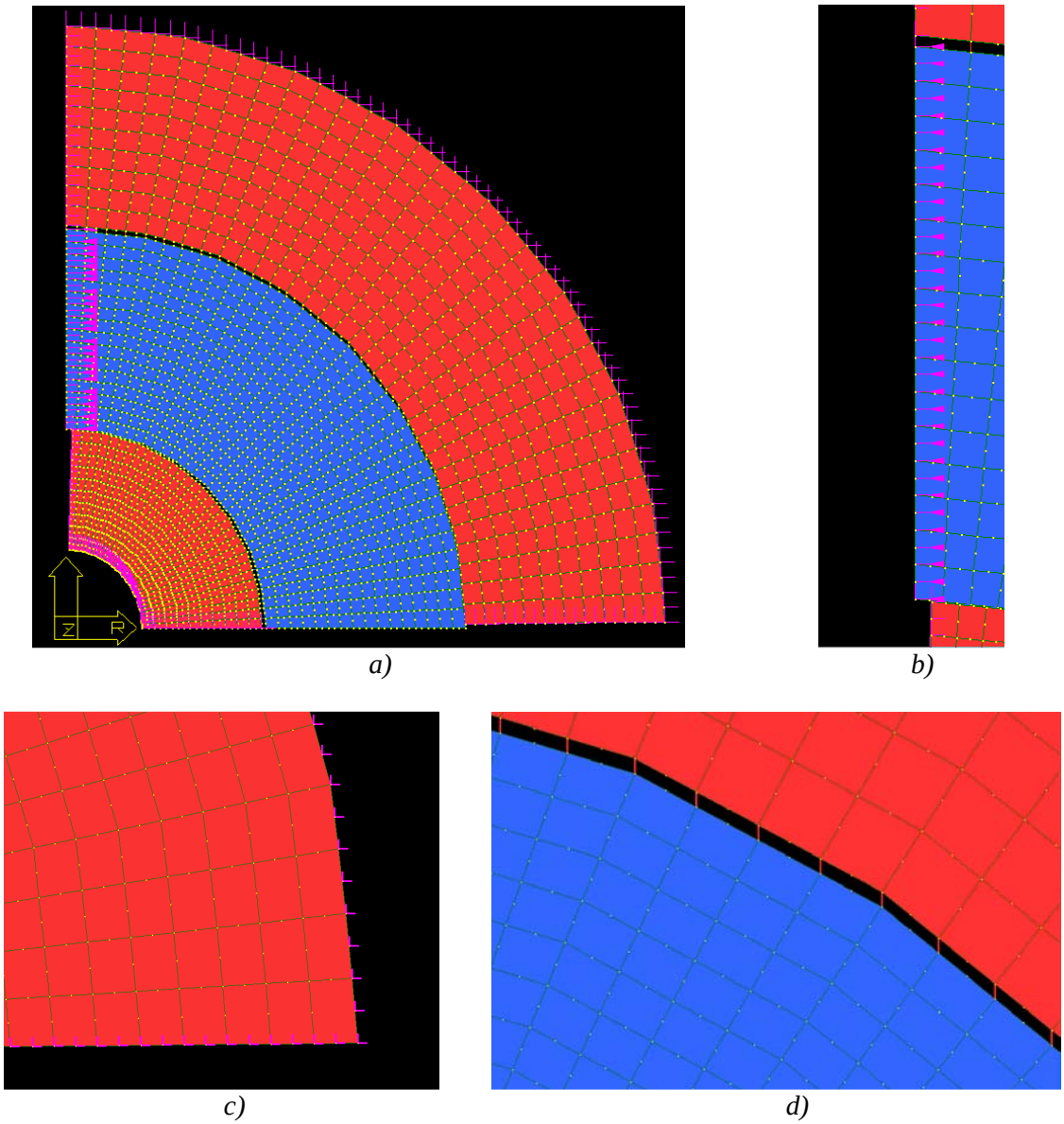

Fig. 4.8 *Overall FEM plates model (a) with draw attention to the load condition (b), matrix boundary restrains (c) and fibre-matrix interface restrains (d)*

The finite elements used for the matrix and the fibre description are 8-noded quadratic 2D plane strain elements. The mesh is shown in Fig. 4.8a. To create the model, a cylindrical coordinate system was used. The load applied at the end of the fibre is represented by assigning displacements along the horizontal direction (Fig. 4.8b), whereas the other end is free. The elements that simulate the cementitious matrix, illustrated in red in Fig. 4.8, are restrained along the outlined external' border (Fig. 4.8c). The matrix' restrains are in the horizontal and vertical direction, they block the node translation but not its rotation. Node-to-node contact elements without friction were used to reproduce the fibre-matrix interface (Fig. 4.8d). These elements are vertically oriented in the fibre upper part and

horizontally oriented in the lower part. This different orientation allows a better simulation of the fibre-matrix contact because it reproduces the real fibre movement inside the channel created in the cementitious matrix.

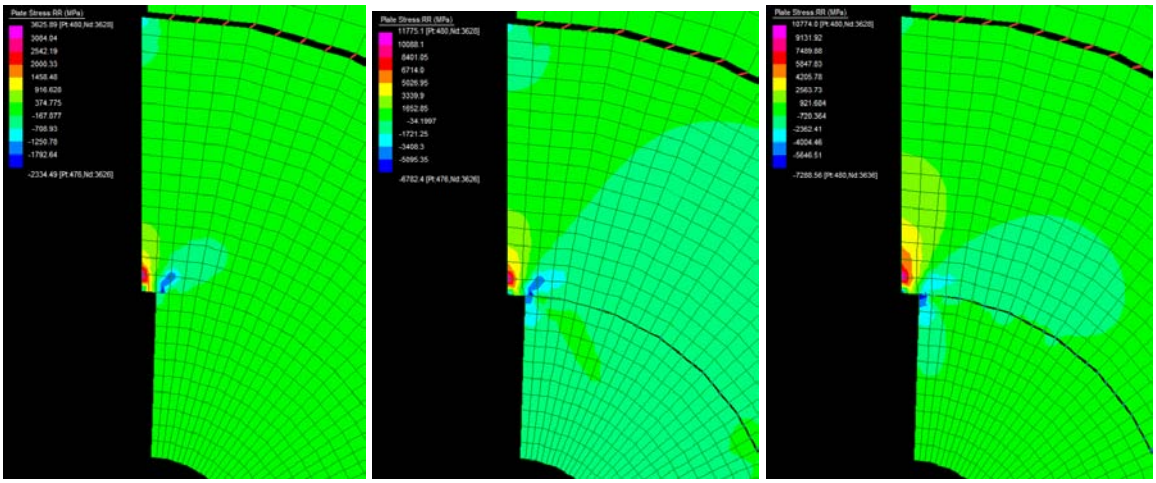

a) *b)* *c)*

Fig. 4.9 *Fibre radial stress distribution with different Young's modulus; 30000 MPa (a), 300000 MPa (b), 3000000 MPa (c)*

The results confirm the stress concentration at the start of the hook. This concentration occurs even with different matrix Young's modulus values are used. When Employing high values of matrix Young's modulus (Fig. 4.9c) it is possible to distinguish the area with higher stress value. This happens because the difference in stress values for the others cases (Fig. 4.9a,b) is too small for the software because it changes the contour stress colour. Furthermore the values confirm the assumptions of a plastic hinge that develops at the start of the hook. In fact, the bigger the difference between the fibre and matrix Young's modulus the more pronounced the stress concentration zone is. Even if this FEM model is not thorough for the overall pull-out test explanation, it is helpful for the problem understanding.

4.3 Pull-out analytical model

4.3.1 Model's algorithm

The analytical model developed and presented in section 4.1 was implemented in a Mathcad program. The Mathcad calculation sheet is subdivided in 3 parts:

- INPUT: the input data are the fibre geometry, the material parameters and some further coefficients necessary to consider the concrete deformation
- CALCULATION PART: in this part the main input is the prescribed displacement. The calculation consists in derive the bending moment upon the curvature. Afterwards the plastic moment is used to find the Internal energy through (4.7) that is compared with the external energy (4.13) to find the pul-out force. The straight fibre pull-out force derived by Lin and Li [1] is included here.
- OUTUPUT: the main output is the pull-out force necessary for the given displacement; the graphic part shows the displacement-force prediction.

Because the simple equations do not need an iterative process, the solution time is quite short. This code allows to any circular cross-section geometry to be considered. The longitudinal geometry of the fibre before the pull-out begins is a combination of a straight part and a circular arc.

4.3.1.1 Model input

One of advantages of the proposed is the freedom in choosing the geometry of the cross-section and of the hook. Obviously the main model assumptions are based on the geometry and material proprieties of commercially available steel fibres. It means that different geometries need different model settings. In the proposed model the input data, given in Fig. 4.10 is split in different parts based on the input type.

GEOMETRIC AND MATERIALS VARIABLES

$d_f := 0.7$ fibre diameter $R_h := 1.73$ hook ratio

$f_y := 1100$ $E_f := 210000$ $\varepsilon_y := \frac{f_y}{E_f} = 5.238 \times 10^{-3}$ steel characteristics

$E_m := 30000$ Young's modulus of matrix (MPa)

a)

LENGTH PARAMETERS

$L_f := 8.6$ initial straight fibre segment

$L_h := R_h \cdot (2\pi) \cdot \frac{1}{10} = 1.087$ hook length

$L_r := 2$ final straight fibre length

$L_i := 2.05$ middle straight fibre length

$L_{tot} := L_f + \frac{n_h}{2} \cdot L_h + L_r + L_i = 14.824$

b)

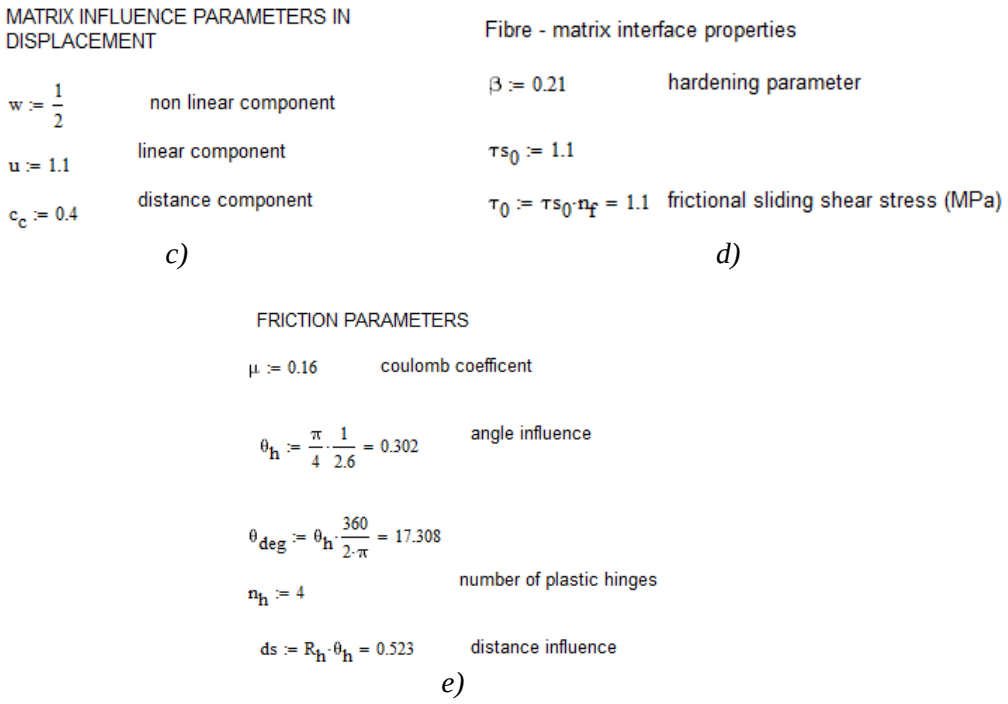

Fig. 4.10 *Models input lines in Mathcad*

A first type (Fig. 4.10a) refers to the material parameters and the geometry of the cross section. The next data batch is about the longitudinal geometry of the fibre (Fig. 4.10b). This model allows to calibrate the matrix deformation through the coefficients in Fig. 4.10c. They modify a set of empirical equations (Fig. 4.12) making sure that the model describes as well as possible the pull-out test. The last two input groups (Fig. 4.10d,e) are needed for the friction and the debonding stage. In particular Fig. 4.10d shows the fibre-matrix interface parameters from the slip-hardening model of Lin and Li [1]. They are the same parameters used for the straight fibres.

4.3.1.2 Model calculation part

The main model input is the fibre displacement "δ", whereas the main output is the pull-out force "P(δ)". Up to the displacement, some equations and parameters might change. These lines of code are shown in Fig. 4.11.

no deformed hook start after the end

$\delta \leftarrow ds \text{ if } ds < \delta < L_r$
$\delta \leftarrow ds + (L_r - \delta) \text{ if } L_r < \delta < (L_r + c_c)$
$n_h \leftarrow n_h - 1 \text{ if } (L_r + c_c) < \delta < (L_r + L_h + c_c)$
$\delta \leftarrow ds \text{ if } (L_r + c_c) < \delta < (L_r + L_h)$
$\delta \leftarrow ds + (L_r + L_h - \delta) \text{ if } (L_r + L_h) < \delta < (L_r + L_h + c_c)$
$n_h \leftarrow n_h - 2 \text{ if } (L_r + L_h + c_c) < \delta < (L_r + L_h + L_i + c_c)$
$\delta \leftarrow ds \text{ if } (L_r + L_h + c_c) < \delta < (L_r + L_h + L_i)$
$\delta \leftarrow ds + (L_r + L_h + L_i - \delta) \text{ if } (L_r + L_h + L_i) < \delta < (L_r + L_h + L_i + c_c)$
$n_h \leftarrow n_h - 3 \text{ if } (L_r + L_h + L_i + c_c) < \delta < (L_r + L_h + L_i + L_h + c_c)$
$\delta \leftarrow ds \text{ if } (L_r + L_h + L_i + c_c) < \delta < (L_r + L_h + L_i + L_h)$
$\delta \leftarrow ds + (L_r + L_h + L_i + L_h - \delta) \text{ if } (L_r + L_h + L_i + L_h) < \delta < (L_r + L_h + L_i + L_h + c_c)$
$\delta \leftarrow 0 \text{ if } \delta > (L_r + L_h + L_i + L_h + c_c)$

four plastic hinges

$\delta \leftarrow ds \text{ if } ds < \delta < (L_r - c_c)$
$\delta \leftarrow ds + (L_r - \delta - c_c) \text{ if } (L_r - c_c) < \delta < L_r$
$n_h \leftarrow n_h - 1 \text{ if } L_r < \delta < (L_r + L_h)$
$\delta \leftarrow ds \text{ if } L_r < \delta < (L_r + L_h - c_c)$
$\delta \leftarrow ds + (L_r + L_h - \delta - c_c) \text{ if } (L_r + L_h - c_c) < \delta < (L_r + L_h)$
$n_h \leftarrow n_h - 2 \text{ if } (L_r + L_h) < \delta < (L_r + L_h + L_i)$
$\delta \leftarrow ds \text{ if } (L_r + L_h) < \delta < (L_r + L_h + L_i - c_c)$
$\delta \leftarrow ds + (L_r + L_h + L_i - \delta - c_c) \text{ if } (L_r + L_h + L_i - c_c) < \delta < (L_r + L_h + L_i)$
$n_h \leftarrow n_h - 3 \text{ if } (L_r + L_h + L_i) < \delta < (L_r + L_h + L_i + L_h)$
$\delta \leftarrow ds \text{ if } (L_r + L_h + L_i) < \delta < (L_r + L_h + L_i + L_h - c_c)$
$\delta \leftarrow ds + (L_r + L_h + L_i + L_h - \delta - c_c) \text{ if } (L_r + L_h + L_i + L_h - c_c) < \delta < (L_r + L_h + L_i + L_h)$
$\delta \leftarrow 0 \text{ if } \delta > (L_r + L_h + L_i + L_h)$

no deformed hook start before the end

$\delta \leftarrow ds \text{ if } ds < \delta < (L_r - c_c)$
$\delta \leftarrow ds + (L_r - \delta - c_c) \text{ if } (L_r - c_c) < \delta < L_r$
$n_h \leftarrow n_h - 2 \text{ if } L_r < \delta < (L_r + L_h + L_i)$
$\delta \leftarrow ds \text{ if } L_r < \delta < (L_r + L_h + L_i - c_c)$
$\delta \leftarrow ds + (L_r + L_h + L_i - \delta - c_c) \text{ if } (L_r + L_h + L_i - c_c) < \delta < (L_r + L_h + L_i)$
$n_h \leftarrow n_h - 3 \text{ if } (L_r + L_h + L_i) < \delta < (L_r + L_h + L_i + L_h)$
$\delta \leftarrow ds \text{ if } (L_r + L_h + L_i) < \delta < (L_r + L_h + L_i + L_h - c_c)$
$\delta \leftarrow ds + (L_r + L_h + L_i + L_h - \delta - c_c) \text{ if } (L_r + L_h + L_i + L_h - c_c) < \delta < (L_r + L_h + L_i + L_h)$
$\delta \leftarrow 0 \text{ if } \delta > (L_r + L_h + L_i + L_h)$

Fig. 4.11 *Code referring to the description of the longitudinal geometry of the fibre*

The lines in Fig. 4.11 explain that the longitudinal geometry could be subdivide in different sections. In particular this model foresee the formation of several plastic hinges along the fibre. The number of plastic hinges is upon the longitudinal geometry of the fibre. For fibre type Dramix (Fig. 4.12) the model predicts the formations of 4 plastic hinges.

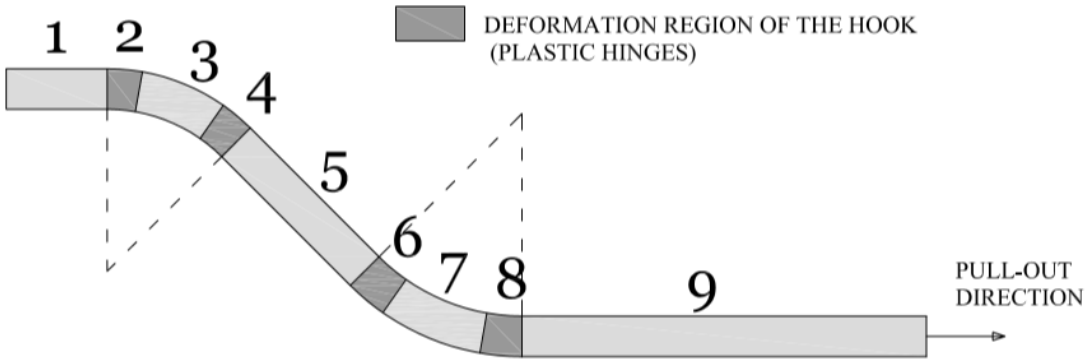

Fig. 4.12 *Dramix fibre longitudinal geometry*

To describe the longitudinal fibre's geometry there are used three displacement depending analysis. The first analysis describes the force-displacement relationship if all the plastic hinges are developed. The second analysis is used at the hooks or straight part end to

describe the incomplete plastification of the cross-section located at the start of the hook. The last one is used as a plastic hinges counter. The three different types of longitudinal geometry description are shown in Fig. 4.11. The use of one instead of another depends on the considered geometry and on the applied assumptions.

As describe in the relations (4.5), (4.6) and (4.7) it is needed the cross section plastic area, hence "x", to achieve the internal energy. But "x" depends by the curvature $1/R_R$. For this reason an empirical relationship was found to correlate the displacement "δ" with the radius of curvature "R_R" (Fig. 4.13).

$$R_R \leftarrow \frac{R_h \cdot \left(ds^w + u\,\delta\right)}{\delta^w + u\,\delta}$$

Fig. 4.13 *Empirical relationship between the displacement "δ" and the curvature radiusR_R*

The empirical equation above is calibrated through the parameters "w" and "u". They are present and can be set in their own input part (Fig. 4.10c). As it is shown in Fig. 4.13 when δ=0 the deformation is null, whereas when δ=ds the hook is completely straightened. "ds" is called the influence distance in the input line (Fig. 4.10e) because it partially represents the matrix deformation.

The algorithm takes into account that for a low value of bending moment, the fibre has only elastic deformation. As explained in section 4.1.2, the algorithm calculates two different types of bending moment energy, depending on the value of "x". If x>R the energy is completely elastic (4.8), otherwise the total energy is the sum of the elastic and plastic energy as shown in (4.7).

Another important aspect is the transfer of the pull-out force along the hook. To consider this transfer, a mechanical relationship proposed by Zile [10] was used. In the Mathcad code the force transfer is considered together with the residual plastic hinges counter in the summary shown in Fig. 4.14.

$$P1(\delta) \leftarrow \left[2f_y \cdot \frac{Ay1(\delta)}{\frac{d_f}{2}}\left(\frac{\frac{d_f}{2}}{R_R} - \frac{\varepsilon_y}{2}\right) + \frac{M_p(\delta)^2}{2 \cdot E_f \cdot (2I)^2} \cdot 2I2(\delta)\right] \cdot \sum_{n=1}^{n_h} e^{\mu \cdot \theta_h \cdot n}$$

$$P2(\delta) \leftarrow \left(\sqrt{\frac{P1(\delta)}{R_h} \cdot M_p(\delta)} \cdot \right) \cdot \sum_{n=1}^{n_h} e^{\mu \cdot \theta_h \cdot n}$$

Fig. 4.14 *Hook counter and force transfer in the calculation part*

The hook counter is used to describe the reducing of the number of plastic hinges during the fibre pull-out. In refer to Fig. 4.12 when the fibre is at the beginning of the pull-out the fibre end is located in the section n°1 and the number of plastic hinges is 4 (n°2/4/6/8). Once the pull-out length overcome the sections 1+2 displacement the number of plastic hinges is reduced to 3 (n° 4/6/8). This regular reduction is take in account by the hook counter. This relation (Fig. 4.14) depends on the friction parameters (Fig. 4.10e) and is a summation because it considers the residual plastic hinges number.

4.3.1.3 Model's output

The model output is the pull-out force. The displacement control could be set to analyze the overall pull-out phenomenon or just the first branch. For the second case, more interesting in the practical application, the displacement steps are smaller. It is even possible to use a load control and obtain the displacement for prescribed pull-out forces. An iterative process is needed to obtain the solution because the equations are highly non linear.

4.3.2 Comparison of model results

The model output was compared with two series of experimental data [10]. These experiments consist in a single fibre pull-out test. Thus was taken a concrete specimen with one embedded fibre. Subsequently the fibre was pulled-out with displacement control. The resultant graph was a force-displacement relationship as Fig. 4.15a. The data have different values of geometry and materials. Two different set of experimental data were considered; the first set was used to calibrate the main parameters of the model and the second one was used validate it. The two different set of fibre parameters are showed in table 4.2 that refer to the Fig. 1.8.

Table 4.2 *Experimental data main fibre parameters*

Fibre type	**σ_y [MPa]**	**r [mm]**	**l_e [mm]**	**l [mm]**	**ρ [mm]**	**θ [rad]**	**Embedded length [mm]**
HE 75/50	1100	0.35	2.00	2.05	1.73	0.62	30
HE+ 1/60	1400	0.45	1.89	1.36	2.23	0.66	25

The comparison between the analytical model results and the experimental data is shown in Fig. 4.14. The vertical axis represents the pull-out force (N), whereas the horizontal axis represents the displacement of the fibre (mm).

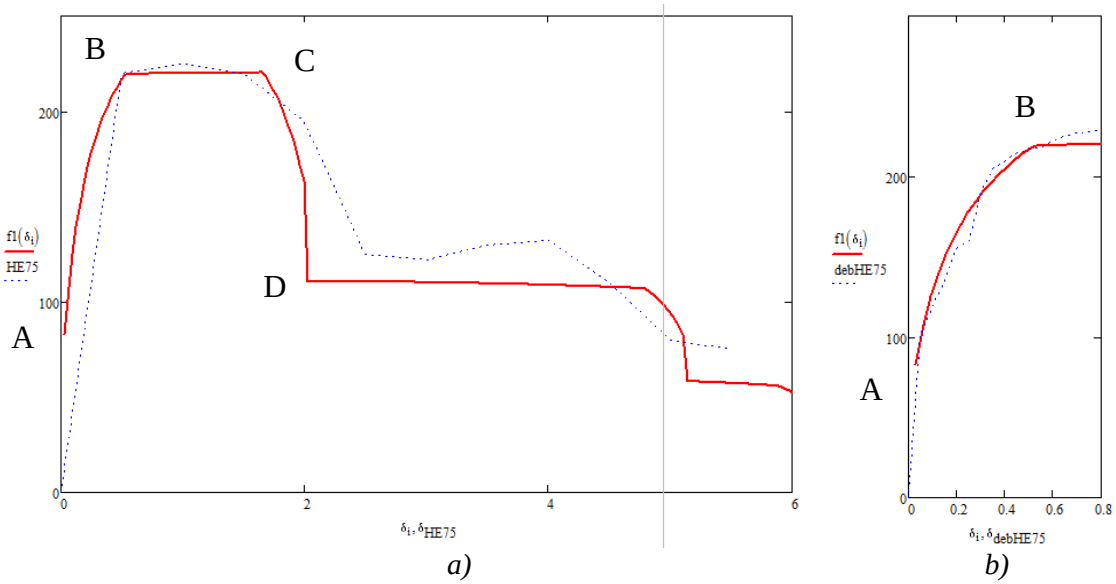

Fig. 4.15 *Analytical model comparison with HE 75/50 fibre experimental data; complete fibre pull-out (a) and first branch displacement (b)*

The model captures the characteristic response observed in the experimental test (Fig. 4.15a). The A-B non linear branch correspond to the situation when all plastic hinges develop. The shape of this section, as well as the displacement, depends upon the input parameters shown in Fig. 4.10c. The maximum force predicted by the model is very similar to the experimental one. The presence of the big step in the force-displacement pull-out curve (section C-D) is due to the fact that as the fibred is pulled out, the number of plastic hinges reduced from four (Fig. 4.12 n°2/4/6/8) to two (Fig. 4.12 n°6/8). This jump occurs when the fibre final straight part reaches the position where the start of the hook was before the pull-out began (l_e length). Beyond this displacement the residual two plastic hinges contribution is constant until the fibre end reach the other hook beginning (Fig. 4.12 between n°5 and n°6). The last two hook plastic hinges subsequently disappear, one at a time, in the final pull-out stage. Through the coefficients w, u and c_c calibration (Fig. 4.10c) even the section A-B (Fig. 4.15b) has a good fit with the experimental data. For comparison even the regular plastic hinges number reduction case is proposed (Fig. 4.15c).

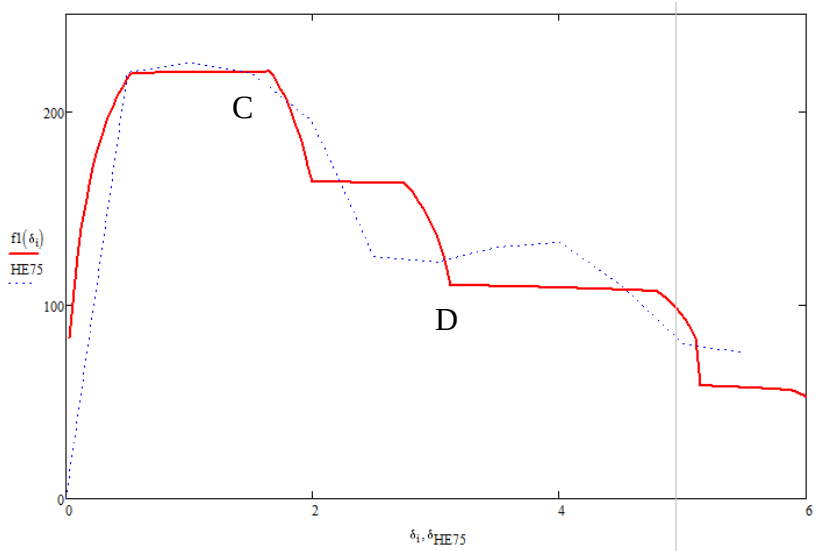

Fig. 4.15c *Analytical model comparison with four plastic hinges reduction*

In the case above the 2 steps in the section C-D do not reproduce accurately the general trend. It is probably due to the geometry of the fibre (Table 4.2 HE 75/50). It does not allow the complete hinge to develop. This is probably because in reality the cementitious matrix deforms around the hook/this region due to the fact that locally, bending stiffness of the hook is higher than that of the straight section of the fibre. As a result the hook does not reach complete straightening.

To validate the model only the geometrical and material proprieties of the fibres were modified and all the calibration coefficients were kept unchanged.

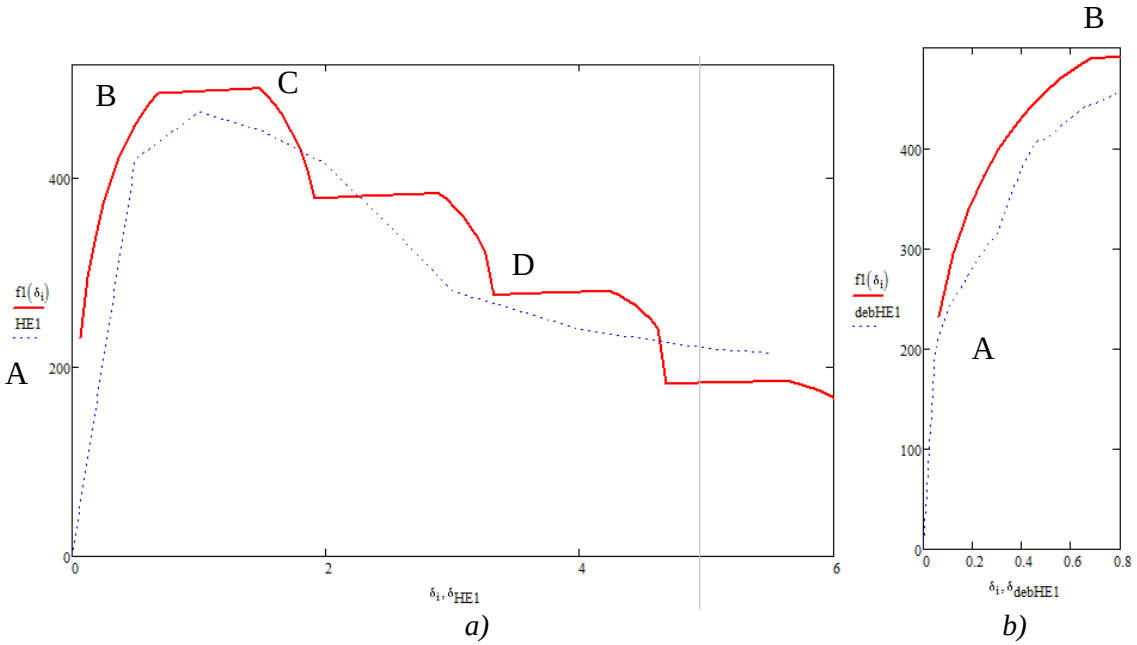

a) *b)*

Fig. 4.16 Analytical model comparison with HE+ 1/60 fibre experimental data; complete fibre pull-out (a) and first branch displacement (b)

For the second set of exeperimental data the model uses progressive reduction of plastic hinges, thus from 4 (n°2/4/6/8) to 3 (n°4/6/8) to 2 (n°6/8) to 1 (n°8), and the fit is better (Fig. 4.16a). The slight slope of the descending's branch is due to the more compact fibre's geometry. It means there is not regular and separate 4 plastic hinges developed. This is because the concrete deformation smoothes the general descending behaviour. Even about the section A-B behaviour the fit is quite satisfying (Fig. 4.16b). In that case the model gives experimental data over extimation. Results obtained from the previous case, when the number of plastic hinges reduces from four to two, are also compared aginst experimental data (Fig. 4.16c).

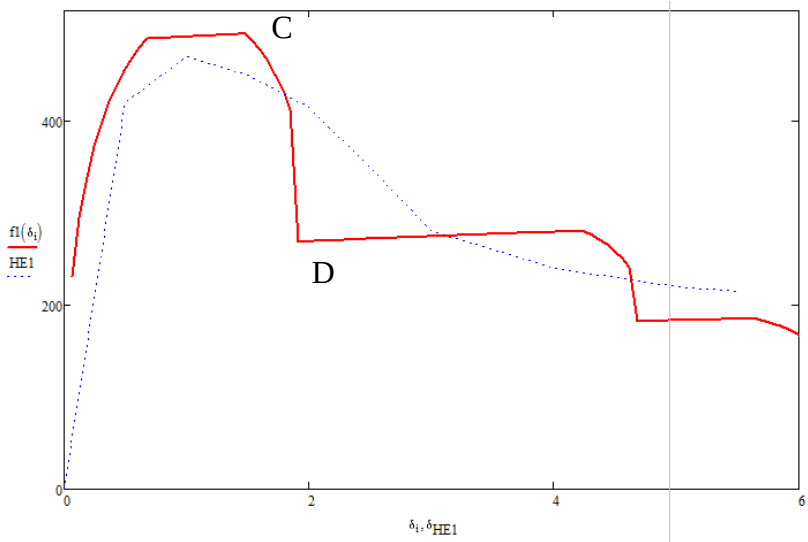

Fig. 4.16c *Analytical model comparison with from four to two plastic hinges reduction*

It can be seen from Fig. 4.16c that the model employing the assumptions mentioned earlier, provides a poorer fit of the experimental data. The stepped post-peak response, attributed to the reduction of the number of plastic hinges, is not distinguishable in the experiments. The area under the force-displacement curve is quite important because it is directly linked with material energy absorption capacity. As explained in the first chapter, one of the main benefits by FRC is a more ductile behaviour or increasing toughness, which becomes extremely important in the case of structures subjected to earthquake loading. Thus a FRC model has to simulate as best as possible the ductile behaviour.

Conclusion

With this thesis many aspects of FRC have been clarified. In particular about FRC with smooth ends was validate the Lin and Li analytical model. It is represented by slip-hardening friction behaviour in the matrix-fibre interface. The overall model is led by few parameters (Table 1.1 and Table 3.3). They describe the fibre geometry and the slip-hardening behaviour. These parameters were studied and their influence in the model has been clarified. In particular the slip-hardening's parameters are quite independent, thus they allow good model control and fit. An important study about the fibre probability distribution and orientation led to some important considerations. In particular two others fibre orientation probability functions were tested. The results showed that the different probability distribution's function doesn't change a lot the model trend. The main effect is about the fibres number the model considers. No correlation between type of fibre probability distribution function and model's parameters was found. Nevertheless bibliography research led to confirm the influence of other parameters. Unfortunately these parameters are not controllable by the model. These parameters are binder dimension, casting flow direction and aggregate shape/dimension. No relationship was found between the volume fraction and the probability density distribution functions. The linear probability density distribution function's analysis allows to change the main angle easily. Thus it is possible better calibrate the orientation angle's distribution, hence the model. About the last studies, it was done something new, but not still enough to whole understanding of the fibres distribution and orientation inside cementitious matrix. To describe the fibre orientation and distribution are needed many factors. This fact makes difficult find statistic function able to represent the random fibre distribution. Nevertheless, to improve the fibre orientation and distribution knowledge some experiments and studies should be made. Particular focus should be used to find relation between the mains fibre parameters and the fibre distribution and orientation. Instead most of the studies are about boundary condition, thus always completely different in the practical work.

The second part of this thesis develops an analytical model to describe the hooked end fibre pull-out test. It is particular interesting because a different and new approach was

used. In particular for this model the small deformation theory and particular assumptions were used. Even if the before hypothesis are quite limitative, the comparison with experimental data confirm the goodness of the model. A great aspect is given by the numerical implementation without iterative resolution or functions approximation. The simple FEM model creation with the commercial software Straus drawn attention to the phenomenon complexity and reproduction. Nevertheless the FEM model was enough good to describe or clarify some particulars aspects. In particular the beam model confirmed the internal work's energy relation. The external work keeps in account even the contact friction component at the fibre beginning. This fact is relevant because this friction force was considered after that the FEM analysis showed its importance. At the treatise's end the double comparison with experimental data confirms the made assumptions goodness. This model was completely developed with the small deformations assumptions and the theory. It is positive because allow a good problem control and understanding. Even the functions implementation is not too complex even because it presents rather simple equations. Nevertheless the results are satisfying, it could be taken like start point for a more complex and refined hooked end fibre pull-out model. The main key-points for the model improving are:

- to consider non linear material (plastic hardening)
- to use the big displacement theory
- to keep in account even the pull-out force tension in the stress distribution
- to create better relation for the main friction contact force
- to keep in account the concrete deformation relationship

All these aspects make the model implementation more complex and probably it will be difficult to implement without iterative solution. If the complexity increase obviously it enhance the force-displacement relationship precision. Another this model's particularity is the simple integration in a crack bridging model impossibility. For this reason the next step in the model develops should be a model fit with polynomial functions (so regular, continues and easy to integrate). It allows to create a constitutive law to insert in a FEM code for FRC materials.

Bibliography

[1] Zhong Lin, Li Victor (1997). *Crack bridging in fiber reinforced cementitious composites with slip-hardening interfaces*. J. Mech. Phys. Solids, Vol. 45, No. 5, Uni. of Michigan, pp. 763-787.

[2] Khaled Marar, Ozgur Eren, Ibrahim Yitem. *Compression specific toughness of normal steel fiber reinforced concrete (NSSFRC) and high strength steel fiber reinforced concrete (HSSFRC)*. Material research, 2011, 14(2) , European Uni. of Lefke and European Mediterranean University , pag. 239-247

[3] L.G.Sorelli, A. Meda, G.A. Pellizari. *Bending and uniaxial tensile test on concrete reinforced with hybrid steel fibers*. Journal in material for civil engineer 2005, 17, Uni. of Brescia and Uni. of Bergamo, pag. 519-527

[4] Zhao H.L., Wang Y., Song T.L., Su H.M.. *Fibre debonding and pull-ot of elastic matrix*. Luoyang institute of science & technology, Henan Six architecture construction group, Sanmenxia city municipal engineering office.

[5] Naaman A.E., Namur G.G., Alwan J.M., Najm H.S.. *Fiber pullout and bond slip 1: analytic study*. Journal of Structural engineering, 1991, 117, Uni. of Michigan, dep. of civil engineering. Pag. 2797-2790

[6] Li V.C., Wang Y., Backer S.. *A micromechanical model of tension-softening and bridging toughening of short random fiber reinforced brittle matrix composites*. Journal of mechanic and physic of solids, Vol 39, (5), Uni. Of Michigan, Georgia institute of technology and Massachusetts institute of technology. Pag. 607-625

[7] Iulia C. Mihai, *Micromechanical constitutive models for cementitious composite materials*. PhD thesis, School of Engineering Cardiff University

[8] Zongjin Li, Faming Li, Tse-Yung Paul Chang, Yiu Wing Mai. *Uniaxial tensil behaviour of concrete reinforced with randomly distributed short fibers*. ACI Materials journal / September-October 1998, pag. 564-574

[9] Jiaping Liu, Changfeng Li, Jianzhong Liu Zhaojin Du, Gong Cui. *Characterization of fibre distribution in steel fiber reinforced cement composites with low water-binder ratio*. State key laboratory of high performance civil engineering materials, Jiangsu research institute of building science. Indian journal of Engineering & material sciences, December 2011, pp. 449-457.

[10] Edmundus Zile, Olga Zile. *Modelling the pullout of hooked steel fibers from cementitious matrix*. Institute of polymer mechanics of the university of Latvia. 4th international conference on integrity, reliability and failure.

[11] Kyriaki Georgiadi-Stefanidi, Euripidis Mistakidis, Dafni Pantuosa, Michalis Zygomalas. *Numerical modelling of the pull-out of hooked steel fibres from high-strength cementitious matrix, supplemented by experimental results*. Laboratory of structural analysis and design, Dept. of civil engineering, university of Thessaly; Institute of steel structures, Aristotle institute of Thessaloniki. Construction and building materials 24 (2010) pag. 2489-2506

[12] Carl Redon, Victor C. Li, Fellow, Cynthia Wu, Hideki Hoshiro, Tadashi Saito and Atsuhisa Ogawa. *Measuring and modifying interface properties of PVA fibers in ECC matrix*. Dept. of Civ. and Envir. Engrg., Univ. Of Michigan, Industrial Goods Development Dept., Kuraray Co., Ltd., Okayama Plant. Journal of materials in civil engineering 2001 pag. 399-406

[13] Victor C. Li. *Postcrack scaling relations for fiber reinforced cementitious composites*. Dept. of Civ. and Envir. Engrg., Univ. Of Michigan. Journal of materials in civil engineering 1992 pag. 41-57

[14] Naaman A.E. and Shah S.P. *Pull-out mechanism in steel fibre-reinforced concrete*. Uni. of Michigan, dep. of civil engineering. Journal of the structural Division 1976 pag 1537-1548

[15] Su-Tae Kang, Jin Keun Kim. *Numerical simulation of the variation of fiber orientation distribution during flow molding of ultra high performance cementiotious composites*. Department of civil engineering, Deagu university, Department of civil and environmental engineering, Korea advanced institute of science and technology. Caement and concrete composites 2012 pag. 208-217.

Appendix I

The model equations (2.12/13/14) derive from the integration of the below:

$$\tilde{\sigma}_B = \frac{\sigma_B}{\sigma_0} = \frac{8}{\pi\tau_0(L_f/d_f){d_f}^2}\int_{\phi=0}^{\pi/2}\int_{z\prime}^{z_0 cos\phi} P(\delta)\, sin\phi\, dz'\, d\phi \qquad \text{(I.1)}$$

with

$$\sigma_1 = \frac{1}{2}\tau_0 V_f(L_f/d_f) \quad \text{and} \quad z' = z/(L_f/2) \qquad \text{(I.2)}$$

and P(δ) depending by the pull-out stage (2.3 - 2.4).

If re-express the embedment length L in terms of L_f, the centroidal location z and the orientation angle φ as:

$$L = \frac{L_f}{2} - \frac{z}{cos\phi} \qquad \text{(I.3)}$$

we can re-write the (2.7) as $z_0 \cdot \cos\varphi$ where:

$$z_0 = 1 - \frac{1}{k}\cosh^{-1}(1 + \frac{\beta\delta}{2d_f}) \quad ; \quad k = \frac{\omega L_f}{2d_f} \quad ; \quad z' = \frac{z}{(L_f/2)} \qquad \text{(I.4)}$$

therefore (I.1), for the debonding stage, became:

$$\tilde{\sigma}_B(\delta)|_{debonding} = \frac{8}{\pi\tau_0(L_f/d_f){d_f}^2}\int_{\phi=0}^{\pi/2}\int_{z\prime=0}^{z_0 cos\phi} P(\delta)\, sin\phi\, dz'\, d\phi \qquad \text{(I.5)}$$

$$\tilde{\sigma}_B(\delta)|_{slipping} = \frac{8}{\pi\tau_0(L_f/d_f){d_f}^2}\int_{\phi=0}^{\pi/2}\int_{z_0 cos\phi}^{(1-\tilde{\delta})cos\phi} P(\delta)\, sin\phi\, dz'\, d\phi \qquad \text{(I.6)}$$

where P(δ) is done by (2.3)

and, for the pull-out stage, became:

$$\tilde{\sigma}_B(\delta)|_{slipping} = \frac{8}{\pi\tau_0(L_f/d_f){d_f}^2}\int_{\phi=0}^{\pi/2}\int_{z\prime=0}^{(1-\tilde{\delta})cos\phi} P(\delta)\, sin\phi\, dz'\, d\phi \qquad \text{(I.7)}$$

where P(δ) is done by (2.4).

The integral was solved just in dz' with the purpose of demonstrate the independence of sinφ by the rest of the integral through the comparison with the Li solution.

About the debonding stage the solution steps are shown below:

$$\tilde{\sigma}_B(\delta)|_{debonding} = \frac{8}{\pi\tau_0(L_f/d_f){d_f}^2}\int_{z\prime=0}^{z_0 cos\phi} \frac{\pi d_f \tau_0(1+\eta)}{\omega}\sqrt{\left(1+\frac{\beta\delta}{2d_f}\right)^2 - 1}\; dz'$$

$$= \frac{2g(1+\eta)}{k}\left[1 - \frac{1}{k}\cosh^{-1}\left(1 + \frac{\beta\delta}{2d_f}\right)\right] \cdot \sqrt{\left(1 + \frac{\beta\delta}{2d_f}\right)^2 - 1} \qquad \text{(I.8)}$$

$$\tilde{\sigma}_B(\delta)|_{slipping} = \frac{8}{\pi\tau_0(L_f/d_f)d_f{}^2}\int_{z_0 cos\phi}^{(1-\tilde{\delta})cos\phi} \frac{\pi d_f \tau_0(1+\eta)}{\omega}\left[\sinh\left(\frac{\omega L}{d_f}\right) + \sinh\left(\frac{\omega(\delta-\delta_0)}{d_f}\right)\right] +$$
$$\pi\tau_0\beta(1+\eta)(\delta-\delta_0)\big(L-(\delta-\delta_0)\big)\,dz' \qquad \text{(I.9)}$$

Thus with the relative substitutions and neglecting cosφ because doesn't depend by dz':

$$= \frac{8}{\pi\tau_0(L_f/d_f)d_f{}^2}\pi\tau_0(1+\eta)\int_{z_0}^{(1-\tilde{\delta})}\frac{d_f{}^2}{\omega}\left[\boxed{\sinh\left(\frac{\omega L_f}{d_f 2}(1-z')\right)}_{\mathbf{A}} + \boxed{\sinh\left(\frac{\omega L_f}{d_f 2}\left(\delta' - \frac{\delta_0}{L_f/2}\right)\right)}_{\mathbf{B}}\right] +$$
$$\beta(\boxed{\delta L}_{\mathbf{C}} - \delta^2 + \boxed{2\delta\delta_0}_{\mathbf{D}} - \boxed{\delta_0 L}_{\mathbf{E}} - \boxed{\delta_0{}^2}_{\mathbf{F}})\,dz' \qquad \text{(I.10)}$$

The subdivision in secondary integrals is clever because most of them are nulls so it allow to simplify very soon a big part of the overall integral:

$$A \to 0 \;;\; B \to 0 \;;\; C \to \frac{\delta}{2k^2}\frac{L_f}{2} \;;\; D \to 0 \;;\; E \to 0 \;;\; F \to 0 \qquad \text{(I.11)}$$

To reach these results some assumptions were done:

- A: $\cosh\big(k(1-z')\big) \sim 1 + \frac{(k(1-z\prime))^2}{2!}$ Taylor series until the 2nd term

  $\left[\cosh^{-1}\left(1 + \frac{\beta\delta}{2d_f}\right)\right]^2 \sim 0$

- B: $k\tilde{\delta} \ll 1 \sim 0$

  $\sinh\left[-\frac{\omega 2}{\beta}[\cosh(k(1-z')) - 1]\right] \sim 0$

- C: $\tilde{\delta}^2 \sim 0$

- D: $\sinh\big(k(1-z')\big) \sim k(1-z')$ Taylor series until the 1st term

  $\tilde{\delta}^2 \sim 0$

- E: $\cosh\big(k(1-z')\big) \sim 1 + \frac{(k(1-z\prime))^2}{2!}$ Taylor series until the 2nd term

  $\tilde{\delta}^2 \sim 0$

- F: $\sinh\big(k(1-z')\big) \sim k(1-z')$ Taylor series until the 1st term

(I.12)

About the post-debonding stage:

$$\tilde{\sigma}_B(\delta) = \frac{8}{\pi\tau_0(L_f/d_f)d_f{}^2}\int_{z'=0}^{(1-\tilde{\delta})cos\phi}\frac{\pi d_f\tau_0(1+\eta)}{\omega}\left[\sinh\left(\frac{\omega L}{d_f}\right)+\sinh\left(\frac{\omega(\delta-\delta_0)}{d_f}\right)\right]+\pi\tau_0\beta(1+\eta)(\delta-\delta_0)\left(L-(\delta-\delta_0)\right)dz' \quad (I.13)$$

Thus with the relative substitutions and neglecting cosφ because doesn't depend by dz':

$$=\frac{8}{\pi\tau_0(L_f/d_f)d_f{}^2}\pi\tau_0(1+\eta)\int_{z'=0}^{(1-\tilde{\delta})}\frac{d_f{}^2}{\omega}\left[\underbrace{\sinh\left(\frac{\omega L_f}{d_f 2}(1-z')\right)}_{A}+\underbrace{\sinh\left(\frac{\omega L_f}{d_f 2}\left(\delta'-\frac{\delta_0}{L_f/2}\right)\right)}_{B}\right]+\beta(\underbrace{\delta L}_{C}-\delta^2+\underbrace{2\delta\delta_0}_{D}-\underbrace{\delta_0 L}_{E}-\underbrace{\delta_0{}^2}_{F})\,dz' \quad (I.14)$$

$$A \rightarrow \frac{k}{2}(1-\tilde{\delta})^2 \;;\; B \rightarrow 0 \;;\; C \rightarrow \frac{L_f}{2}\frac{1}{2}\delta(1-\tilde{\delta})^2 \;;\; D \rightarrow 0 \;;\; E \rightarrow 0 \;;\; F \rightarrow 0 \quad (I.15)$$

Even to reach these results some assumptions were done:

- A: $\sinh\left(k(1-z')\right) \sim k(1-z')$ Taylor series until the 1st term

  $\tilde{\delta}^2 \sim 0$

- B: $k\tilde{\delta} \ll 1 \sim 0$

  $\sinh\left[-\frac{\omega 2}{\beta}[\cosh(k(1-z'))-1]\right] \sim 0$

- C: $\tilde{\delta}^2 \sim 0$

  add and deduct $\tilde{\delta}^2$; $\tilde{\delta}$

- D: $\sinh(k) \sim 0$

  $\tilde{\delta}^2 \sim 0$

- E: $\cosh\left(k(1-z')\right) \sim 1+\frac{(k(1-z'))^2}{2!}$ Taylor series until the 2nd term

  $\sinh\left(k(1-z')\right) \sim k(1-z')$ Taylor series until the 1st term

  $\tilde{\delta}^2 \sim 0$

- F: $\sinh\left(k(1-z')\right) \sim k(1-z')$ Taylor series until the 1st term

(I.16)

Appendix II

The fibre orientation part inner the whole integral is describe by:

$$\int_0^{\frac{\pi}{2}} \sin\emptyset \cos\emptyset \, e^{f\emptyset} \, d\emptyset \tag{II.1}$$

after a double integration for part it results:

$$\int_0^{\frac{\pi}{2}} \sin\emptyset \cos\emptyset \, e^{f\emptyset} \, d\emptyset = \frac{1}{(4+f^2)} (e^{f\pi/2} + 1) \tag{II.2}$$

And, if we keep in account the definition in (2.20), we can write:

$$\frac{g}{2} = \frac{1}{(4+f^2)} (e^{f\pi/2} + 1) \tag{II.3}$$

For the solution of the constant distribution integral (3.2) is possible bring out of the integral the constant parameter 2/π, therefore the integral became:

$$\int_0^{\frac{\pi}{2}} \cos\emptyset \, e^{f\emptyset} \, dz' d\emptyset \tag{II.4}$$

After a double integration for part the integral has the analytic solution below

$$\frac{(e^{f\pi/2} - f)}{(1+f^2)} \tag{II.5}$$

The solution of the linear distribution (3.6) pass for the decomposition of the linear equations in 3 integrals:

$$\underbrace{\int_0^{\emptyset_2} m_1 \emptyset \cos\emptyset \, e^{f\emptyset} \, d\emptyset}_{\mathbf{F1}} + \underbrace{\left[\int_{\emptyset_2}^{\emptyset_3} m_2 \emptyset \cos\emptyset \, d\emptyset}_{\mathbf{F2}} + \underbrace{\int_{\emptyset_2}^{\emptyset_3} a_2 \cos\emptyset \, d\emptyset\right]}_{\mathbf{F3}} \tag{II.6}$$

Where F1 and F2 are different just for the m constant and F3 is the same , hence:

F1=F2 $\rightarrow$ $\int \emptyset \cos\emptyset \, e^{f\emptyset} \, d\emptyset = \sin\emptyset \, \emptyset \, e^{f\emptyset} - \int \underbrace{\sin\emptyset \, e^{f\emptyset} f\emptyset}_{\mathbf{A}} + \underbrace{\sin\emptyset \, e^{f\emptyset}}_{\mathbf{B}}$

$$\rightarrow m\left[\frac{e^{f\emptyset}}{(1+f^2)} \cdot \left(\sin\emptyset \cdot \emptyset + \cos\emptyset \cdot (1 + f\emptyset)\right) - \frac{2fe^{f\emptyset}}{(1+f^2)^2} \cdot (\sin\emptyset + f\cos\emptyset)\right] \tag{II.7}$$

Where:

A $\rightarrow$ $f \cos\emptyset \, e^{f\emptyset} - f^2 \int \cos\emptyset \, e^{f\emptyset}$

B $\rightarrow$ $f\left[-f \cos\emptyset \, e^{f\emptyset} + \int f \cos\emptyset \, e^{f\emptyset} + \int \cos\emptyset \, e^{f\emptyset}\right]$

(II.8)

Appendix III

The circle shape integration needs, for the internal energy definition, some particular attentions. It is due to the particular geometric shape, it is not common in civil engineering field. Below they are describe some geometric definition necessary for the internal energy relation.

$$\theta_0 = 2\,\mathrm{acos}\left(\frac{x}{R}\right) \tag{III.1}$$

$$R_R = \frac{x}{\varepsilon_y} \tag{III.2}$$

$$\varepsilon_y = \frac{f_y}{E} \tag{III.3}$$

$$\varepsilon_p = \frac{R}{R_R} \tag{III.4}$$

They derive from linear theory and geometric relations. In particular they describe the relationship between curvature and linear strain distribution. In the lines below are shown the geometric expressions used to calculate tension and stress for a circle shape. These expression are referred to Fig. I.1.

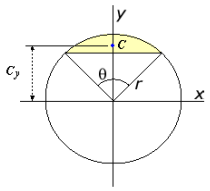

C_x	C_y	Area
0	$\frac{4r}{3}\left(\frac{\sin^3\frac{\theta}{2}}{\theta-\sin\theta}\right)$	$\frac{r^2}{2}(\theta-\sin\theta)$

Moment of Inertia about the *x* axis I_x	Moment of Inertia about the *y* axis I_y	Polar Moment of Inertia about the *z* axis J_z
$\frac{r^4}{8}\left(\theta-\sin\theta+2\sin\theta\sin^2\frac{\theta}{2}\right)$	$\frac{r^4}{24}\left(3\theta-3\sin\theta-2\sin\theta\sin^2\frac{\theta}{2}\right)$	$\frac{r^4}{4}\left(\theta-\sin\theta+\frac{2}{3}\sin\theta\sin^2\frac{\theta}{2}\right)$

Fig. I.1 Geometric meaning of circle parameters

Circle segment area:

$$A1 = \frac{1}{2}R^2(\theta_0 - sin\theta_0) \tag{III.5}$$

Circle segment branch:

$$b1 = \frac{4}{3}R\frac{\left[sin\left(\frac{\theta_0}{2}\right)\right]^3}{\theta_0 - sin\theta_0} \quad \text{(III.6)}$$

circle segment inertia moment:

$$I1 = \frac{R^4}{8}\left(\theta_0 - sin\theta_0 + 2sin\theta_0\left[sin\left(\frac{\theta_0}{2}\right)\right]^2\right) \quad \text{(III.7)}$$

Circle segment $\int y\ dx\ dy$:

$$Ay1 = \frac{2}{3}R^3\left[sin\left(\frac{\theta_0}{2}\right)\right]^3 \quad \text{(III.8)}$$

Half circle inertia moment:

$$I = \frac{\pi R^4}{8} \quad \text{(III.9)}$$

Half circle inertia moment minus circle segment inertia moment:

$$I2 = I - I1 \quad \text{(III.10)}$$

Half circle (indeed with $\theta = \pi$) minus circle segment $\int y\ dx\ dy$:

$$Ay2 = \frac{2}{3}R^3\left(sin\left(\frac{\pi}{2}\right) - \left[sin\left(\frac{\theta_0}{2}\right)\right]^3\right) \quad \text{(III.11)}$$

Ay2 arm, it was calculate like I2/Ay2 (like the baricenter definition Sy/A):

$$b2 = \frac{3}{16}R\frac{\pi - \left[\theta_0 - sin(\theta_0) + 2sin(\theta_0)\left[sin\left(\frac{\theta_0}{2}\right)\right]^2\right]}{sin\left(\frac{\pi}{2}\right) - \left[sin\left(\frac{\theta_0}{2}\right)\right]^3} \quad \text{(III.12)}$$

Once it defines the geometric relationship it is possible calculate the plastic moment through the formula force times arm.

Force given by the circle segment, so area (A1) times yield tension (f_y):

$$F1 = A1f_y \quad \text{(III.13)}$$

Force given by the rest of the half circle area. In the formula, tensions has linear behaviour so it is used A2y/x (where 1/x is to no-dimension the integral):

$$F2 = A2y\frac{f_y}{x} \quad \text{(III.14)}$$

The final moment is simply force times branch (it is times 2 because the integrals above are referee just to half circle section)

$$Mp = 2(F1\ b1 + F2\ b2) \quad \text{(III.15)}$$

The relationship for the friction component considers geometric relation (III.16) and cantilever static scheme with punctual force (III.17).

$$P_{\perp}R = P\ ds \qquad \text{(III.16)} \qquad\qquad P_{\perp} = \frac{M}{ds} \qquad \text{(III.17)}$$

If it replaces the definition of "ds" from (III.16) in (III.17) it finds the orthogonal force formula below:

$$P_{\perp} = \sqrt{\frac{P}{R}M} \qquad \text{(III.18)}$$

(No) Thanks

I will not thank Prof. Bernhard Schrefler and Prof. Tony Jefferson because their availability and kindness brought together this collaboration that led me to write my thesis in Cardiff, making me believe to have obtained a good knowledge of the English.

I surely will not thank my supervisor Iulia because she gave me such an interesting thesis topic that made me work nonstop, gladly off cause, thus it took me away from the parties. Furthermore she mentored me and taught me, making me believe to have a good knowledge of the argument.

even the family doesn't deserve a thank you because, supporting me and encouraging me in that experience, made me spend a long time far away from home

I absolutely will not thank my flatmates and everybody I met during that period for all the amazing parties and dinners that destroyed the house. For all the unforgettable and awesome nights that made me come home drunk and taught me how to cook making me believe that even l am a decent cook

last but not least I will not thank my friends in Italy especially those who came to Cardiff because they didn't forget me thus making me feel homesick and as a result my time spent in Cardiff was tough at times.